

DTIC FILE COPY

2

AD-A200 114

# NAVAL POSTGRADUATE SCHOOL Monterey, California



## THESIS

DTIC  
ELECTE  
NOV 08 1988  
S D  
CH

EFFECTS OF IRREGULAR SEA SURFACE  
AND EVAPORATION DUCT ON  
RADAR DETECTION PERFORMANCE

by

Moshe Marom

June 1988

Thesis Advisor:

R. Janaswamy

Approved for public release; distribution is unlimited

88 11 08 026

UNCLASSIFIED

SECURITY CLASSIFICATION OF THIS PAGE

AD-800 114

## REPORT DOCUMENTATION PAGE

1a REPORT SECURITY CLASSIFICATION <b>UNCLASSIFIED</b>			1b RESTRICTIVE MARKINGS		
2a SECURITY CLASSIFICATION AUTHORITY			3 DISTRIBUTION/AVAILABILITY OF REPORT Approved for public release; distribution is unlimited		
2b DECLASSIFICATION/DOWNGRADING SCHEDULE					
4 PERFORMING ORGANIZATION REPORT NUMBER(S)			5. MONITORING ORGANIZATION REPORT NUMBER(S)		
6a NAME OF PERFORMING ORGANIZATION Naval Postgraduate School		6b OFFICE SYMBOL (If applicable) 62	7a. NAME OF MONITORING ORGANIZATION Naval Postgraduate School		
6c ADDRESS (City, State, and ZIP Code) Monterey, California 93943-5000			7b. ADDRESS (City, State, and ZIP Code) Monterey, California 93943-5000		
8a NAME OF FUNDING SPONSORING ORGANIZATION		8b. OFFICE SYMBOL (If applicable)	9. PROCUREMENT INSTRUMENT IDENTIFICATION NUMBER		
8c. ADDRESS (City, State, and ZIP Code)			10. SOURCE OF FUNDING NUMBERS		
		PROGRAM ELEMENT NO.	PROJECT NO.	TASK NO.	WORK UNIT ACCESSION NO.
11 TITLE (Include Security Classification) <b>EFFECTS OF IRREGULAR SEA SURFACE AND EVAPORATION DUCT ON RADAR DETECTION PERFORMANCE</b>					
12 PERSONAL AUTHOR(S) <b>MAROM, Moshe</b>					
13a TYPE OF REPORT <b>Master's Thesis</b>		13b TIME COVERED FROM TO		14. DATE OF REPORT (Year, Month, Day) <b>1988 June</b>	15 PAGE COUNT <b>93</b>
16. SUPPLEMENTARY NOTATION The views expressed in this thesis are those of the author and do not reflect the official policy or position of the Department of Defense or the U.S. Government.					
17 COSATI CODES			18 SUBJECT TERMS (Continue on reverse if necessary and identify by block number)		
FIELD	GROUP	SUB-GROUP	sea surface, roughness, lobing factor, refractivity, evaporation, detection, low altitude targets		
19 ABSTRACT (Continue on reverse if necessary and identify by block number) The detection performance of microwave search radars operating in close proximity to the sea surface is evaluated. The effects of media characteristics on the propagation of electromagnetic waves have been incorporated. Specular and diffused scattering from a rough surface, and the effects of the curvature of the earth's surface have been included in the study. Additionally, surface ducting effects caused by atmospheric anomalies are presented. Some design and operational considerations which can improve the detection performance of a surface search radar, are also presented.					
20 DISTRIBUTION/AVAILABILITY OF ABSTRACT <input checked="" type="checkbox"/> UNCLASSIFIED/UNLIMITED <input type="checkbox"/> SAME AS RPT <input type="checkbox"/> DTIC USERS			21. ABSTRACT SECURITY CLASSIFICATION <b>UNCLASSIFIED</b>		
22a NAME OF RESPONSIBLE INDIVIDUAL <b>JANASWAMY, R.</b>			22b TELEPHONE (Include Area Code) <b>408-646-3217</b>		22c OFFICE SYMBOL <b>62Js</b>

DD FORM 1473, 84 MAP

83 APR edition may be used until exhausted  
All other editions are obsolete

SECURITY CLASSIFICATION OF THIS PAGE

U.S. Government Printing Office: 1986-506-24.

UNCLASSIFIED

Approved for public release; distribution is unlimited

Effects of Irregular Sea Surface and Evaporation Duct on Radar Detection  
Performance

by

Moshe Marom  
Cdr., Israeli Navy  
B.Sc. in Electrical Engineering, Technion-Israel  
Institute of Technology, Haifa, Israel, 1979

Submitted in partial fulfillment of the  
requirements for the degree of


MASTER OF SCIENCE  
IN ELECTRICAL ENGINEERING

from the

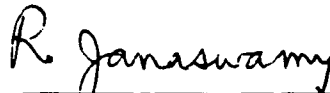
NAVAL POSTGRADUATE SCHOOL

June 1988

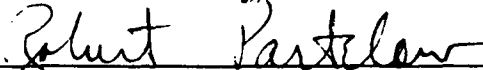
Author:

  
Moshe Marom

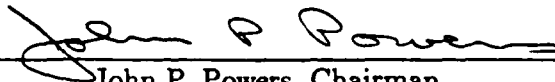
Approved by:



Rama Janaswamy, Thesis Advisor



Robert Partelow, Second Reader



John P. Powers, Chairman

Department of Electrical and Computer Engineering



Gordon E. Schacher  
Dean of Science and Engineering

## ABSTRACT

The detection performance of microwave search radars operating in close proximity to the sea surface is evaluated. The effects of media characteristics on the propagation of electromagnetic waves have been incorporated. Specular and diffused scattering from a rough surface, and the effects of the curvature of the earth's surface have been included in the study. Additionally, surface ducting effects caused by atmospheric anomalies are presented. Some design and operational considerations which can improve the detection performance of a surface search radar, are also presented.



Accession For	
NTIS GRA&I	<input checked="checked" type="checkbox"/>
DTIC TAB	<input type="checkbox"/>
Unannounced	<input type="checkbox"/>
Justification	
By	
Distribution/	
Availability Codes	
Dist	Avail and/or Special
A-1	

## TABLE OF CONTENTS

I.	INTRODUCTION . . . . .	1
	A. MOTIVATION OF STUDY . . . . .	1
	B. SCOPE OF WORK . . . . .	1
	C. ORDER OF WORK . . . . .	2
II.	RAYLEIGH CRITERION AND FRESNEL ZONES FOR SURFACE ROUGH- NESS . . . . .	4
	A. INTRODUCTION . . . . .	4
	B. ANALYTICAL MODEL AND CONSIDERATIONS . . . . .	4
	1. Surface Roughness: General Definition . . . . .	4
	2. Fundamental assumptions . . . . .	5
	3. Roughness Criteria . . . . .	7
	4. Active Scattering Region . . . . .	8
	a. Fresnel zones dimensions . . . . .	10
	b. Special Practical Cases . . . . .	11
III.	EARTH'S CHARACTERISTICS AFFECTING PROPAGATION . . . . .	14
	A. INTRODUCTION . . . . .	14
	B. SPHERICAL SURFACE AND REFRACTION EFFECTS . . . . .	14
	1. Horizon Range . . . . .	15
	C. COMBINED REFLECTION COEFFICIENT . . . . .	18
	D. REFLECTION COEFFICIENT OF PLANE SMOOTH EARTH . . . . .	20
	E. ILLUSTRATIONS OF REFLECTION COEFFICIENT OF A SMOOTH SURFACE . . . . .	21

F.	THE EFFECT OF SURFACE ROUGHNESS ON THE REFLECTION OF ELECTROMAGNETIC WAVES . . . . .	23
G.	SHADOWING EFFECT . . . . .	30
H.	DEPOLARIZATION . . . . .	31
IV.	LOBING PHENOMENA ANALYSIS . . . . .	35
A.	INTRODUCTION . . . . .	35
B.	MULTIPATH FADING PHENOMENA . . . . .	35
C.	THE LOBING FACTOR . . . . .	37
1.	Applications . . . . .	37
2.	Combined Phase Difference $\alpha$ , and Detecting Range $R_d$ . . . . .	37
D.	PATH DIFFERENCE DERIVATION . . . . .	40
E.	PRACTICAL LOBE FACTOR DERIVATION . . . . .	42
F.	DISCUSSION . . . . .	43
G.	LOBING ANALYSIS FOR TYPICAL CASES . . . . .	45
H.	SUMMARY AND CONSEQUENCES . . . . .	58
V.	ANOMALOUS ATMOSPHERIC PROPAGATION . . . . .	59
A.	INTRODUCTION . . . . .	59
B.	TROPOSPHERIC REFRACTION . . . . .	59
1.	Refraction Effect . . . . .	60
C.	REFRACTION LOSS . . . . .	63
D.	PROPAGATION UNDER ANOMALOUS CONDITIONS . . . . .	65
E.	SURFACE DUCT CHARACTERISTICS AND ATMOSPHERIC RELATIONSHIP . . . . .	68
F.	CONCLUSIONS OF ANOMALOUS PROPAGATION . . . . .	70
VI.	SUMMARY AND CONCLUSIONS . . . . .	71
A.	SUMMARY . . . . .	71

B. CONCLUSIONS AND RECOMMENDATIONS . . . . .	71
APPENDIX: DERIVATION OF ELLIPSES FOR FRESNEL ZONES . . . . .	73
LIST OF REFERENCES . . . . .	75
BIBLIOGRAPHY . . . . .	76
INITIAL DISTRIBUTION LIST . . . . .	77

## LIST OF TABLES

2.1	FRESNEL ZONES AREA $A_1$ . . . . .	12
3.1	PARAMETERS OF SEA STATE. . . . .	30



## LIST OF FIGURES

2.1	Reflected Waves from Perfectly Smooth Surface . . . . .	5
2.2	Reflected Waves from Rough Surface . . . . .	6
2.3	Glistening Zones on a Reflecting Plane . . . . .	9
3.1	Spherical Surface Geometry . . . . .	16
3.2	Divergence by a Convex Surface . . . . .	17
3.3	Incident and Reflected Wave by a Smooth Dielectric Surface . . . . .	22
3.4	Reflection Coefficient of Very Smooth Sea Water . . . . .	23
3.5	Phase of Reflection Coefficient $\phi$ of Very Smooth Sea . . . . .	24
3.6	Reflection Coefficient for Low Depression Angles of Very Smooth Sea . .	24
3.7	Phase of Reflection Coefficient for Low Depression Angle of Very Smooth Sea . . . . .	25
3.8	Dependence of Mean Square of Scattering Coefficient on Phase Variance, for Specular Reflection from Rough Surface . . . . .	29
3.9	Right Circular Polarization Produced by Horizontal and Vertical Polar- izations . . . . .	33
4.1	Multipath Geometry over a Plane Reflecting Surface . . . . .	41
4.2	Vertical Lobe Pattern Caused by a Plane Reflecting Surface. . . . .	44
4.3	Vertical Lobe Pattern for the Same Parameters as Figure 4.2 Except Antenna Height Increased to 20 m. . . . .	47
4.4	Vertical Lobe Pattern for the Same Parameters as Figure 4.2 Except the Frequency is Ten Times Higher (1000 MHz). . . . .	48
4.5	Detection Pattern of Rectangular Antenna with Uniform Field Distri- bution. . . . .	50

4.6	Detection Pattern Same Parameters as Figure 4.5 except Including the Scattering Coefficient Effect. . . . .	51
4.7	Detection Pattern Showing the Effect of Sea Roughness. . . . .	52
4.8	Detection Pattern for Higher Frequency (1000 MHz) and Narrower Vertical Beam Width. . . . .	54
4.9	Effect of Sea Roughness on a 1000 MHz Detection Pattern of a Radar. .	55
4.10	Detection Pattern under Lobing Effect for S Band Naval Surface Searching Radar. . . . .	56
4.11	Received Signal Relative to Minimum Detectable Signal, for Multipath and Free Space Conditions. . . . .	57
5.1	(a) Extension of Radar Horizon; (b) Elevation Angular Error . . . . .	61
5.2	(a) Bent Beam due to Refraction; (b) Straight Line Propagation with Effective Earth Radius $4/3r_e$ . . . . .	62
5.3	Ray Pattern for Refractive Loss Analysis . . . . .	64
5.4	Lens Effect Loss as a Function of Elevation Angle vs. Range . . . . .	65
5.5	Ray Propagation Pattern under Ducting Conditions . . . . .	67
5.6	Relative Received Signal Under Duct and Free Space Conditions. . . . .	69

## LIST OF VARIABLES

$A$	Free space wave front area
$A'$	Refractive wave front area
$A_n$	Area of the $n$ th ellipse
$c$	Velocity of light in free space
$D$	Divergence factor
$d_g$	Geometrical horizon range
$d_o$	Optical horizon range
$d_h$	Radar horizon range
$\hat{d}$	duct thickness
$E_d$	Electric field of direct electromagnetic (EM) wave
$E_r$	Electric field of reflected EM wave
$E_0$	Electric field of free space
$E_x^r$	Receiving electric field in $x$ direction
$E_x^t$	Transmitting electric field in $x$ direction
$E_y^r$	Receiving electric field in $y$ direction
$E_y^t$	Transmitting electric field in $y$ direction
$e$	Water vapor pressure
$F$	Lobing factor
$f_d$	Magnitude of direct pattern factor
$f_r$	Magnitude of reflected pattern factor
$f(\gamma)$	Complex pattern factor
$h_1$	Transmitting antenna height for curved surface
$h'_1$	Transmitting antenna height for plane surface

$h_2$	Target/receiver height for curved surface
$h'_2$	Target/receiver height for plane surface
$k$	Wave number
$\hat{k}$	Effective earth radius factor
$L$	Atmospheric loss
$L'$	Refraction loss
$N$	Normalized index of refraction
$n$	Index of refraction
$N_e$	Index of refraction of earth surface
$N_s$	Exponential index of refraction
$P$	Barometric pressure
$P_r$	Radar receiving power
$R$	Distance, detection range
$\bar{R}$	Surface roughness factor
$R_D$	Diffused scattering coefficient
$R_d$	Direct path ray
$R_0$	Free space range
$R_s$	Specular scattering coefficient
$r_e$	Earth's radius
$r$	Transmitter receiver horizontal distance
$V_g$	Velocity of EM wave
$X_{on}$	Center of $n$ th ellipse
$X_{in}$	Semimajor axis of $n$ th ellipse
$Y_{in}$	Semiminor axis
$\alpha$	Combined phase difference
$\alpha'$	Incident and reflected angle from tilted surface

$\alpha_\beta$	Brewster angle
$\beta_d$	Phase of direct pattern factor
$\beta_r$	Phase of reflected pattern factor
$\Gamma_d$	Horizontal complex reflection coefficient
$\Gamma_r$	Vertical complex reflection coefficient
$\gamma_d$	Elevation angle
$\gamma_r$	Depression angle
$\Delta h$	Mean sea wave height
$\Delta\phi$	Path phase difference
$\delta$	Path difference
$\delta_n$	$n$ th ellipse path difference
$\delta_0$	Approximated path difference
$\bar{\delta}$	Angular separation
$\epsilon$	Dielectric constant of earth
$\epsilon_c$	Dielectric constant for free space
$\epsilon_{rc}$	Relative complex dielectric constant
$\phi_H$	Horizontal polarization phase difference
$\phi_V$	Vertical polarization phase difference
$\sigma$	Conductivity
$\lambda$	EM wavelength
$\mu$	Magnetic permittivity of earth
$\mu_0$	Magnetic permittivity of free space
$\mu_r$	Relative magnetic permittivity
$\rho$	Magnitude of reflection coefficient
$\rho_d$	Magnitude of diffused reflection coefficient

$\rho_s$  Magnitude of specular reflection coefficient  
 $\theta$  Incidence or grazing angle

## ACKNOWLEDGMENT

To my advisor, Professor Rama Janaswamy, I wish to express deep appreciation for his guidance in my work.

Gratitude is also extended to my second reader, Professor Robert Partelow, for his helpful comments.

I am very thankful also to Mrs. Robert Limes for typesetting this document. Her dedication and proficiency produced this fine looking document.

Finally, I thank my wife Ronit for her love, patience, devotion, and inspiration, without which this work could not possibly have been done.

# I. INTRODUCTION

## A. MOTIVATION OF STUDY

Microwave search radars installed on ships, or at shore stations, operating close to the sea surface, have a strong interaction with the propagating medium and the sea. The reflected field is a function of the transmitting frequency, the incidence angle, and the electric properties of the surface boundary. The atmospheric medium also interferes with the electromagnetic wave by refraction, absorption, and attenuation.

The present study tries to evaluate quantitatively the effects of sea roughness and special atmospheric conditions, like ducting, on electromagnetic propagation. It is shown that the propagation is considerably influenced by the media between the radar and the target.

The motivation of analyzing the irregularities of the sea surface with periodic or random variations, together with atmospheric refractivity, is to predict and optimize the detection ranges of a search radar.

## B. SCOPE OF WORK

This study begins by introducing the Rayleigh criterion and the Fresnel zone model for discriminating between a rough and a smooth surface. The specularly reflected wave interferes with the direct propagating wave, resulting in a constructive and destructive interference.

Computation and illustration of detection patterns, depending on radar parameters and sea surface characteristics, are performed. The resulting plots show a strong effect of constructive and destructive interference between the direct and reflected fields.



It is shown that under some special conditions the detection range could be doubled relatively to free space range.

The abnormal propagation caused by strong vertical gradient of tropospheric refractivity, results in a considerably extended horizontal detection range. From conservation of energy point of view, the increased density of energy through one path results in a decreased density through other paths causing "holes" in detection.

The results of this study show that by appropriate design and operation, detection ranges of a radar could probably be improved. Also, the limited detection range could be predicted and optimized.

### C. ORDER OF WORK

Chapter II presents a theoretical study on surface roughness, specular reflection and diffused scattering. The Rayleigh criterion and Fresnel zones for surface roughness are introduced.

Chapter III introduces a simplified model for propagation above a spherical surface. The divergence factor and the reflection coefficient from the sea surface are discussed in detail. The shadowing effect for radar with very low grazing angles, and the depolarization by the reflecting surface are also introduced.

Chapter IV is based on the study of Chapter II and III. This chapter discusses the lobing phenomena. Computer plots of detection contours are illustrated. Conclusions regarding improved detection range for low flying aircraft and surface targets are suggested.

Chapter V introduces abnormal propagation in the atmosphere. The atmospheric conditions for this phenomena to occur, and the effect on radar detection ranges are discussed.

Chapter VI is the summary and conclusion of this study. The Appendix gives an analytical derivation of Fresnel zones.

## II. RAYLEIGH CRITERION AND FRESNEL ZONES FOR SURFACE ROUGHNESS

### A. INTRODUCTION

When an electromagnetic short wave (VHF and above) propagates above the earth's surface, it is affected by the earth's surface and its atmosphere. The reflected field of the electromagnetic wave from such boundaries depends on the angle of incidence, the wavelength and the characteristics of the reflecting plane (conductivity, permittivity, and permeability). The difficulty of qualitatively analyzing the influence of the medium on the propagating wave is due to the fluctuating irregularities of the surface boundaries. These irregularities impose limitations on the performance of communication and radar systems. These random fluctuations of the parameters, defining a practical terrain profile, are the main obstacle in establishing its relationship with the properties of the electromagnetic wave. For this reason the prediction of radar and communication performance is limited. In other words, the effects on propagation introduces degradations in radar performance.

In this chapter we will discuss the theory of *specular reflection* and its effect upon field strength on the assumption that the reflection coefficient of a perfectly smooth earth are known. Effects of surface roughness will also be discussed.

### B. ANALYTICAL MODEL AND CONSIDERATIONS

#### 1. Surface Roughness: General Definition

The first stage in constructing a model for the propagation problem is to analyze and understand the reflecting boundary which is usually varying in position and time, and therefore is not plane.

The basic difference between a rough and a smooth surface is that a smooth surface will reflect the incident plane wave specularly in a single direction, whilst a rough surface will scatter the wave in various directions (see Fig 2.1, 2.2). From this definition one can conclude that the roughness of the surface is determined basically by the angle of incidence and the frequency of the plane wave. A smooth surface is a singular limiting case of a rough one.

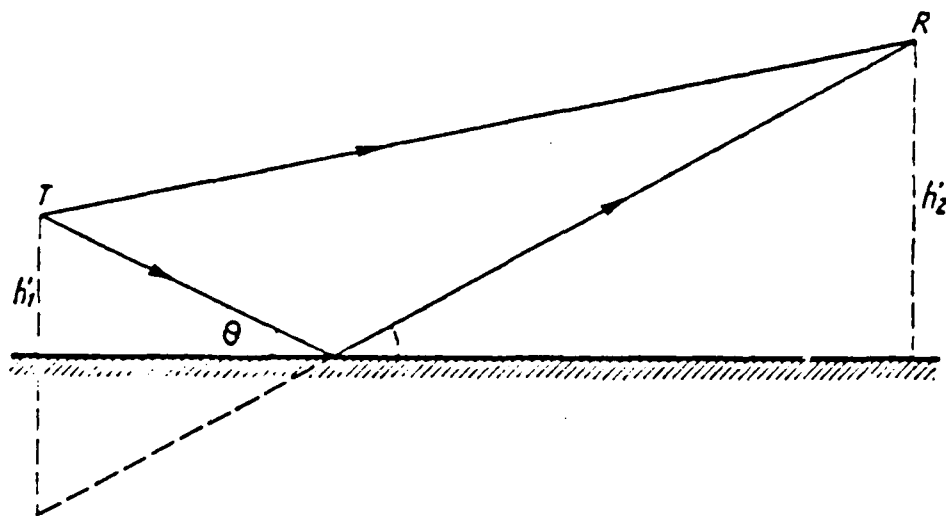


Figure 2.1: Reflected Waves from Perfectly Smooth Surface [Ref. 1].

In Chapters III and IV we will introduce the sea medium which will include the time varying nature of the scattering surface and its effects such as the fading of the received signal by the shape and movement of the water waves [Ref. 3].

## 2. Fundamental assumptions

The empirical and analytical theory of rough surface scatter is usually simplified by some of the following assumptions [after Ref. 3]:

- 1) Far field approximations only.

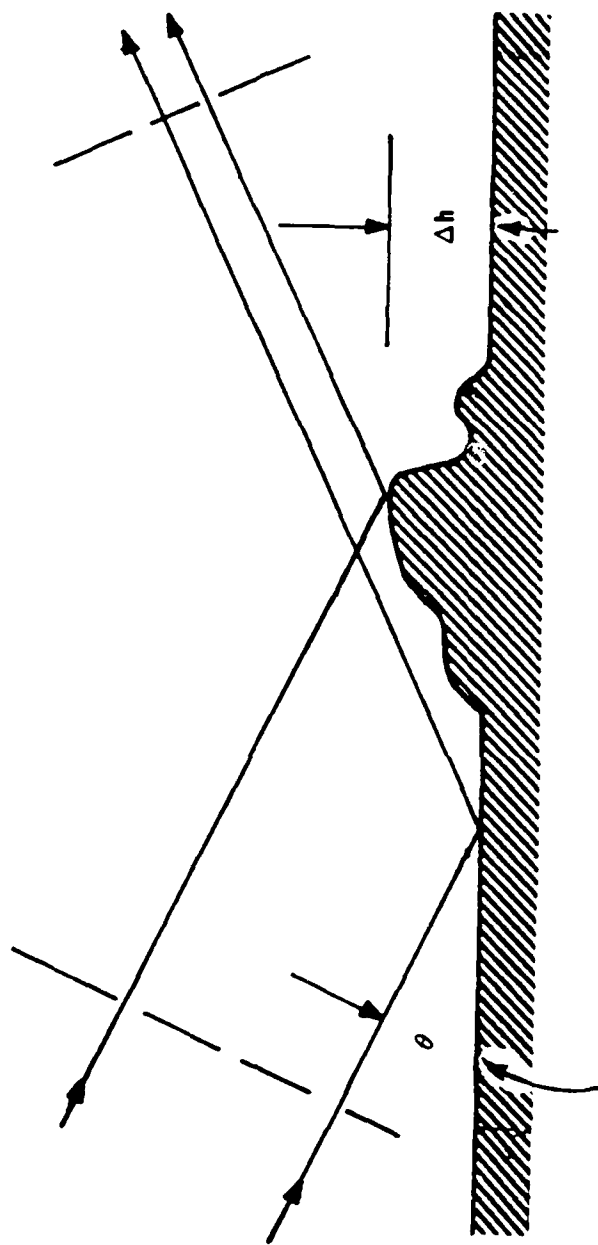


Figure 2.2: Reflected Waves from Rough Surface [Ref. 2].

- 2) Shadowing effects are neglected.
- 3) The radius of curvature of the scattering surface is much larger than the wavelength of the incident wave.
- 4) Multiple scattering is neglected.
- 5) Particular models of surface roughness are restricted (periodic and random).

### 3. Roughness Criteria

As mentioned earlier, the efficiency of *specular reflection* from a rough surface is a function of the ratio of the surface roughness dimensions to the wavelength, and of the grazing angle. We will try to define the values of the grazing angle, the wavelength, and the surface roughness at which the *specular reflection* changes into *diffuse* scattering.

The best known criterion involving these parameters is that of Lord Rayleigh. The path difference between the two waves is

$$\delta = 2\Delta h \sin \theta. \quad (2.1)$$

The phase difference  $\Delta\phi$  corresponding to this path difference is:

$$\Delta\phi = k\delta = \frac{4\pi\Delta h}{\lambda} \sin \theta, \quad (2.2)$$

where  $\lambda$  is the wavelength and the propagation number is given by  $k = \frac{2\pi}{\lambda}$ .

For small phase differences, there is almost no effect by the roughness and the surface behaves as a smooth surface. This can be achieved if  $\frac{\Delta h}{\lambda}$  or  $\theta$  are very small which leads to  $\Delta\phi \approx 0$ . Increasing  $\frac{\Delta h}{\lambda}$  and/or  $\theta$  will increase the phase difference. When the phase difference is equal to  $\pi$  the two waves will be in phase opposition and cancel in that direction. According to conservation of energy, the energy of the electromagnetic wave is scattered in other directions. Thus we conclude that for:

- 1)  $\Delta\phi = 0$       the surface reflects specularly and is smooth.
- 2)  $\Delta\phi = \pi$       the surface scatters and is rough [Ref. 1].

A criterion for discriminating between rough and smooth surfaces is chosen arbitrarily as  $\pi/2$  which is the average phase difference between these two extremes

[Ref. 5]. Thus a surface is considered to be smooth for the height of roughness  $\Delta h$  to be smaller than:

$$\Delta h < \frac{\lambda}{8 \sin \theta}. \quad (2.3)$$

This criterion, sometimes called the Rayleigh criterion, is a simplified argument based on ray theory for describing the irregularities of a surface.

The Rayleigh model excludes, by definition (because of the ray assumption), the case when the roughness of the surface elements are comparable in size to the wavelength of the propagating wave.

The sea surface in such a case usually consists of irregular distributions of sizes and shapes of the waves. An accurate solution in this case requires complex methods not yet developed to satisfy boundary conditions of a random rough surface. However, in the literature, simplifications have been made in order to calculate the effective reflection coefficient, using sea surface models with sinusoidal or wedge shaped waves [Ref. 3].

#### 4. Active Scattering Region

As mentioned above, the complexity of the real surface is so severe that no analytical model can describe it accurately. In this section we will try to consider the effects of scattering in terms of a simple model called the Fresnel zones, or the glistening surface. Ray analysis suggests that reflections would be confined to a small region of the rough surface, which depends on the transmitter receiver configuration.

The glistening surface, or the Fresnel near zones, is defined as that part of a rough surface that reflects a significant amount of electric field of the propagating wave into the receiver, at given heights of the source and the receiver [Ref. 4].

Applying Huygen's principle to the ray theory, one should interpret the reflected ray from a single point on the surface as the fact that an energy source illuminating a large portion of the surface creates currents which radiate in all directions. At any point in space the total field is the sum of the radiation from these currents and

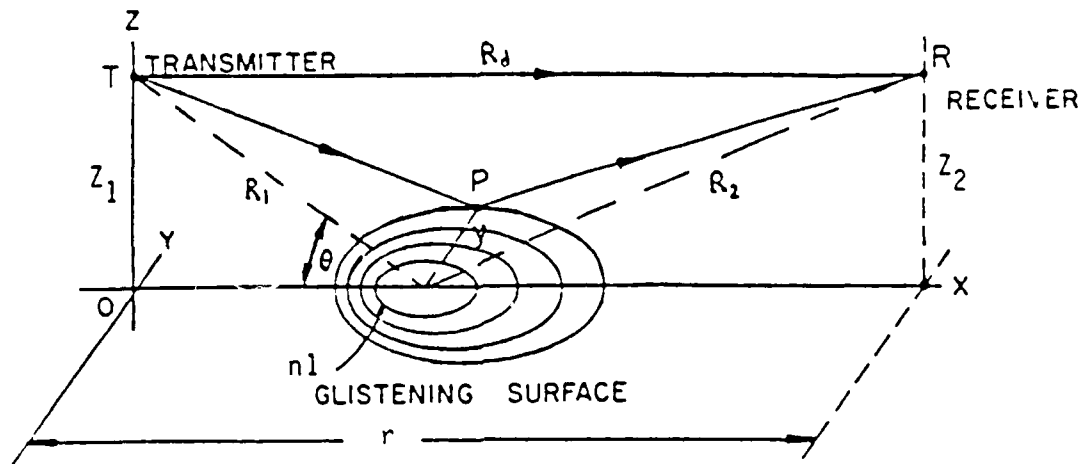


**Figure 2.3: Glistening Zones on a Reflecting Plane [Ref. 4].**

the direct propagating field. Figure 2.3 illustrates a scenario consisting of a transmitter at height  $z_1$  and a receiver at height  $z_2$  operating above a smooth plane.

The direct ray path is  $R_d$  and the indirect path from a point on earth is  $R_1 + R_2$ . As mentioned, the incident field induces currents on the plane  $xy$  which radiate a reflected field. We want to find the zones in which the path difference between the direct and the indirect path is constant and equals to  $\Delta\phi$ . The path difference is [Ref. 1,3]:

$$R_1 + R_2 - R_d = \delta. \quad (2.4)$$

Since the direct path is unchanged and  $\delta$  is constant:

$$R_1 + R_2 = \text{Const.} = R_d + \delta \quad (2.5)$$

Putting the path difference  $\delta$  into phase difference notation:

$$\Delta\phi = \delta \cdot k, \quad (2.6)$$

or

$$\Delta\phi = \frac{\delta \cdot 2\pi}{\lambda}. \quad (2.7)$$



Equation 2.5 is an equation of ellipsoids with  $T$  and  $R$  as foci and the direct path  $R_d$  as axis of revolution (see Figure 2.3). The geometric locus of all points on the  $xy$  plane which intersect with the ellipsoids are ellipses which describe a constant phase difference,  $\Delta\phi$ . In order to describe more zones of other constant path difference we increase  $\delta$ , for instance, by  $\lambda/2$ , or  $\pi$  radians (for phase interpretations).

We find a family of ellipses which describes zones of constant phase. Each zone differs from its adjacent zone by  $\pi$ , so the radiation from two successive zones is in opposite phase. They do not cancel totally because of the slow variation in the amplitude between zones. We shall see that the first zone,  $n = 1$ , is the contributing zone [Ref. 4].

#### a. Fresnel zones dimensions

In order to apply smooth earth phase difference formulas one should know the dimensions of the Fresnel zones, which can give an indication as to what the minimum dimensions of a smooth area should be for these formulas to be valid.

The approximate path difference between the direct path and the geometrical point (only one) of reflection is:

$$\delta_0 \approx \frac{2z_1 z_2}{r}; \quad (2.8)$$

the  $n$ th ellipse path difference is determined by:

$$\delta_n \approx \delta_0 + \frac{n\lambda}{2}. \quad (2.9)$$

By using this approximation and substituting it into Equations A.13, A.15, and A.11 and using the assumptions of Equation A.16 (Appendix A), we find useful formulae for the semiminor axis ( $y_{1n}$ ), the semimajor axis ( $x_{1n}$ ) and the center ( $x_{0n}$ ) of the  $n$ th ellipse:

$$y_{1n} \approx \pm \frac{\sqrt{n\lambda r}}{2} \sqrt{\frac{1 + \frac{2\delta_0}{n\lambda}}{1 + \frac{(z_1+z_2)^2}{n\lambda r}}}, \quad (2.10)$$

$$x_{1n} \approx x_{0n} \pm \frac{r}{2} \frac{\sqrt{1 + \frac{2\delta_0}{n\lambda}}}{\left[1 + \frac{(z_1+z_2)^2}{n\lambda r}\right]} x_{1n} \triangleq x_{0n} \pm \xi_n, \quad (2.11)$$

and

$$x_{0n} \approx \frac{r}{2} \frac{1 + \frac{2z_1(z_1+z_2)}{n\lambda r}}{1 + \frac{(z_1+z_2)^2}{n\lambda r}}. \quad (2.12)$$

The area of the  $n$ th ellipse is:

$$A_n = \pi \xi_n y_{1n}. \quad (2.13)$$

By substituting Equations 2.10 and 2.11 into Equation 2.13, we obtain:

$$A_n = \frac{\pi r}{4} \frac{\sqrt{n\lambda r} (1 + \frac{2\delta_n}{n\lambda})}{(1 + \frac{(z_1+z_2)^2}{n\lambda r})^{3/2}}. \quad (2.14)$$

### b. Special Practical Cases

The minimum area for smooth surface assumption (Fresnel zone) calculated by Equation 2.14 can be simplified for special practical cases of a radar tracking an aircraft:

$$\frac{4z_1}{z_2} \ll 1. \quad (2.15)$$

The height of the radar antenna is  $z_1$  and the height of an aircraft is  $z_2$ . Since the first zone is the most contributing area to the total field received at  $R$  (Fig. 2.3), we should consider only this zone ( $n = 1$ ). At the reflection point for the lowest lobe of the interference pattern,  $r \gg z_1, z_2$  and  $\delta = \frac{\lambda}{2}$ .

The parameters  $y_{1n}$ ,  $x_{1n}$  and  $z_{0n}$  are simplified to [Ref. 4]:

$$y_{11} \approx 2\sqrt{2}z_1 \approx \frac{x_0}{\frac{3\sqrt{2}z_1}{\lambda}}, \quad (2.16)$$

$$x_{11} \approx x_{01} \pm \frac{8\sqrt{2}z_1^2}{\lambda}, \quad (2.17)$$

$$x_{01} \approx \frac{12z_1^2}{\lambda}. \quad (2.18)$$

Two cases are considered to illustrate the dimensions and positions of the first Fresnel zone. In the first case, the range, the height of the source  $z_1$ , and the height of the receiver  $z_2$ , are given and it is required to determine the position and dimensions of the first zone. In the second case  $r$  and  $z_1$  are given and we want to find

dimensions of the first zone. In the second case  $r$  and  $z_1$  are given and we want to find the dimensions and position of the first zone which will produce the reflected wave to form the lowest lobe of the interference pattern for which  $\delta_0 = \frac{\lambda}{2}$ . The calculated values for given grazing angle and mean height of sea waves are given in Table 2.1 [Ref. 3,4].

**TABLE 2.1: FRESNEL ZONES AREA  $A_1$  [REF. 4].**

Parameter	Case 1		Case 2	
$\lambda$ [cm]	10	100	10	100
$r$ [m]	10,000	10,000	10,000	10,000
$z_2$ [m]	1000	1000	2.5	2.5
$z_1$ [m]	100	100	100	100
$\delta_0$	20m	20m	5cm	50cm
$x_{01}$ [m]	910	943	9350	6830
$y_{11}$ [m]	9.1	29	6.6	44
$\xi_1$ [m]	83	262	615	2760
$\theta$ [°]	6.3°	6.3°	0.59°	0.72°
$h_{\max}$ [m]	0.11	1.1	1.22	1.25
$A_1$ [m <sup>2</sup> ]	2,370	23,900	128,000	382,000

Table 2.1 indicates that the minimum areas of the first zone for smooth assumptions seem to be large, and are larger with increasing wavelength. For mean peak to peak wavelength of almost 1m, in case 2, the smooth area for the first lobe of interference is much larger than the smooth area in case 1, especially for short wave lengths.

The contribution of energy to the receiver from each zone is calculated by integrating the current excitation of each zone. Though the successive zones differ in phase by  $\pi$  radians, it is not evident that their contribution to the received energy

cancels out totally and that only the first zone or part of it contributes to the received energy.

The reason for this doubt could be caused by the variation in the amplitude of excitation within a single zone, especially in small grazing angles. From later research it seems that the first Fresnel zone is likely to be the most important zone of contribution to the received energy, together with two other areas near the source and near the receiver which differ from the Fresnel zones.

In this discussion only the phase of the reflected radiation has been considered. We did not consider the conductivity and dielectric constant nor the reflection coefficient. These will be discussed in the next chapter. The sea surface is more complex than the land surface, with time variations in addition to fluctuations in amplitude and phase of the scatterers.

### **III. EARTH'S CHARACTERISTICS AFFECTING PROPAGATION**

#### **A. INTRODUCTION**

After discussing the roughness of the surface in Chapter II and deriving roughness criteria and a model, we want to discuss in this chapter the major characteristics of the earth's surface which will affect the magnitude, phase, and direction of a propagating wave.

Firstly, we will consider the effects of a spherical surface and refraction effects and present a model for horizon propagation range, taking into account the convex shape of the earth's surface. Secondly we will analyze the reflectivity of the surface.

Compared with propagation in free space, the presence of terrain affects the Radar Cross Section (RCS) of scatterers. The reflection from terrain creates an interference pattern which will be discussed in detail in Chapter IV. Also, the terrain casts a shadow which introduces diffraction phenomena. The main outcome will be a reflection coefficient for a rough and a smooth surface, which will define quantitatively the reflected and/or the scattered electromagnetic wave; especially from the sea-surface.

Finally the shadowing and depolarization effects will be introduced. These effects are also significant in determining the reflected and/or scattered field of an electromagnetic propagating wave.

#### **B. SPHERICAL SURFACE AND REFRACTION EFFECTS**

Electromagnetic wave reflectivity becomes more complex when the surface is not flat. The reflected wave is decreased in amplitude; also the phase difference between

propagation over a convex surface. The difference between the plane and spherical surface is that in spherical surface the height of the transmit and receive antennas is increased in order to achieve equivalent line of sight. Figure 3.2 illustrates the reduction in the reflected wave's amplitude towards a specific direction due to the divergence of the waves into a larger area, compared with a flat surface. [Ref. 2]

Realizing that the propagation of the electromagnetic wave is in the atmosphere, one must consider the refraction effect. This effect causes the waves to bend during propagation rather than propagating in straight lines, usually resulting in an extension of the maximum range of propagation. It is convenient to analyze the effect of the phenomena together with the earth's curvature. Detailed discussion on atmospheric refraction is carried out in Chapter V.

### 1. Horizon Range

The reduced heights ( $h'_1, h'_2$ ) of the radar and target for a plain surface are calculated by:

$$h'_1 = h_1 - \frac{d_1^2}{2\hat{k}r_e}, \quad (3.1)$$

and

$$h'_2 = h_2 - \frac{d_2^2}{2\hat{k}r_e}, \quad (3.2)$$

where  $d_1$  is the curved radar horizon when  $h'_1$  is zero,  $d_2$  is the curved distance from the reflecting point to the receiving antenna and  $h_1$  and  $h_2$  are the actual heights of the transmitting and receiving antennas respectively (see Figure 3.1). The average effect of standard atmospheric refraction is interpreted by increasing the earth radius  $r_e$  by the factor  $\hat{k} = 4/3$ . (For more details see Chapter V.) The differences in heights of the radar antenna and the target, due to refraction and earth curvature, are given by [Ref. 2]:



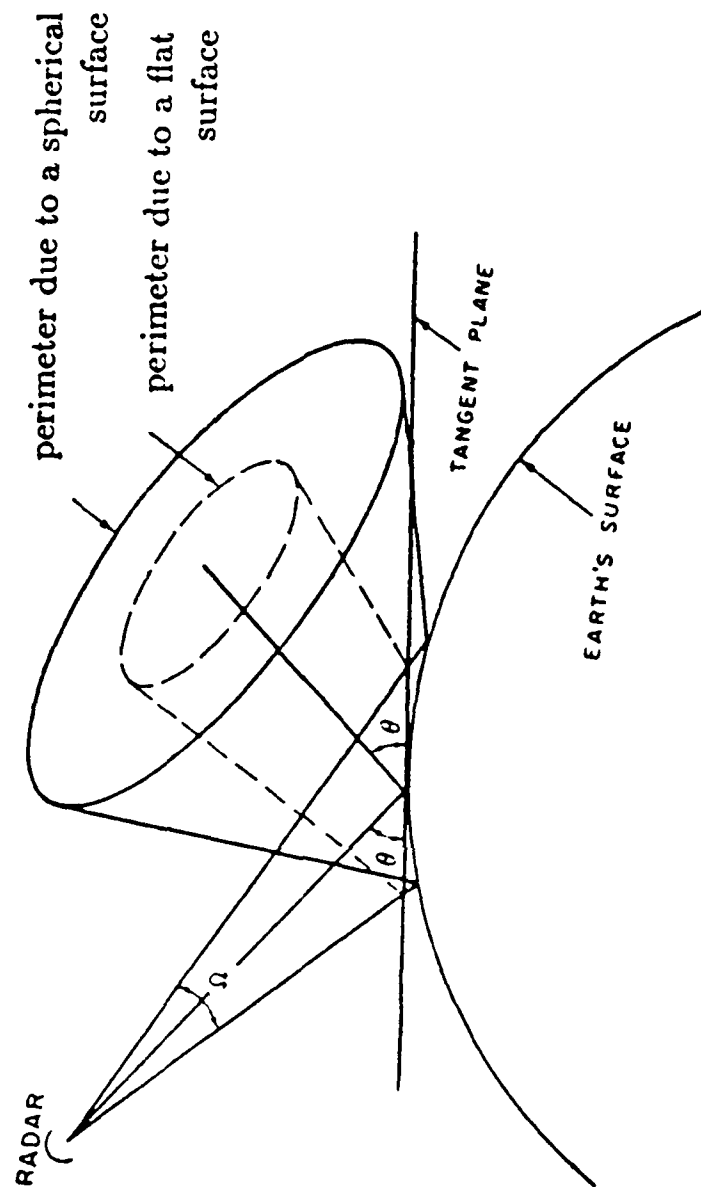


Figure 3.2: Divergence by a Convex Surface [Ref. 2].



$$\Delta h_{1,2} = \frac{d_{1,2}^2}{2}. \quad (3.3)$$

The radar horizon  $d_h$  is given by:

$$d_h = \sqrt{2\hat{k}r_e h_1 + h_1^2} + \sqrt{2\hat{k}r_e h_2 + h_2^2}. \quad (3.4)$$

The distance  $d_1 + d_2$  is the horizon range of the radar if  $h_2$  is zero. Using this fact in Equation 3.3, the horizon range then can be approximated to:

$$d_h \approx \sqrt{2\hat{k}r_e h}, \quad (3.5)$$

where  $h$  is the antenna height of the radar and  $\hat{k}r_e$  is the effective earth radius. For standard atmospheric conditions ( $\hat{k} = 4/3$ ) the distance  $d_h$  has the form of:

$$d_h = 1.23\sqrt{h \text{ (ft)}} \quad \text{in nautical miles.} \quad (3.6)$$

Furthermore, the relationship between the optical, radar and geometric (propagating along perfect straight lines) horizons for standard atmosphere is: [Ref. 8]

$$d_h = 1.07d_o = 1.15d_g, \quad (3.7)$$

where  $d_h$ ,  $d_o$  and  $d_g$  are the radar, optical, and geometrical horizon ranges. Equation 3.7 stresses that under standard conditions the radar horizon range is 7% larger than the optical horizon and 15% larger than the geometric horizon. In abnormal conditions such as ducting, the electromagnetic waves can propagate to longer ranges due to diffraction from the earth, combined with refraction from atmospheric layers. [Ref. 2]

### C. COMBINED REFLECTION COEFFICIENT

As mentioned above the physical principle which allows radar coverage to be extended beyond the geometrical horizon is divergence or refraction. The electromagnetic wave is diffracted around the earth's curvature, the range of propagation depends

on the frequency. The larger the wavelength (lower frequency) the more the wave is propagated, due to refraction.

This phenomena is applied in VLF (Very Low Frequency) for world-wide communications. Since radar frequencies have short wavelengths compared with earth dimensions, only small amounts of energy will be diffracted, resulting in insufficient propagation beyond the radar horizon by divergence. [Ref. 5]

The combined reflection coefficient of earth is determined by three factors:

- 1)  $D$ , the divergence factor that describes the reduction in reflection due to earth's curvature (see Figure 3.2),
- 2)  $\rho$ , the reflection coefficient of a plane smooth surface, and,
- 3)  $\bar{R}$ , a factor which defines the surface roughness.

The combined reflection coefficient is the product of the three factors mentioned above [Ref. 2]:

$$\left\{ \begin{array}{l} \text{combined} \\ \text{reflection} \\ \text{coefficient} \end{array} \right\} = \rho D \bar{R}. \quad (3.8)$$

The factor  $\rho$  may be calculated from Fresnel's equations (see next section). The factor  $\bar{R}$  is equal to unity if the surface is smooth. If the surface is extremely rough  $\bar{R}$  is equal to zero. The factor  $D$  varies between 0 and 1, and  $D$  approaches unity when:

- 1)  $h_1$  or  $h_2$  (Figure 3.1) approaches zero or  $\hat{k}$  becomes very large (especially over water), and,
- 2) For radar geometry such that the earth can be assumed flat [Ref. 2].

The divergence coefficient  $D$  is given by:

$$D \simeq \left[ 1 + \frac{2d_1 d_2}{\hat{k} r_e d_h \sin \theta} \right]^{-1/2}, \quad (3.9)$$

where  $\theta$  is the grazing angle.

#### D. REFLECTION COEFFICIENT OF PLANE SMOOTH EARTH

Prior to discussing the characteristics of reflection of a plane wave from rough surface, one should first consider the reflection characteristics from a smooth surface. The relative complex dielectric constant  $\epsilon_{rc}$  is given by:

$$\epsilon_{rc} = \frac{\epsilon}{\epsilon_0} - 60i\lambda\sigma, \quad (3.10)$$

where  $\epsilon_0$  is the dielectric constant of free space,  $\lambda$  is the wavelength in meters,  $\sigma$  is the conductivity in  $mho - m^{-1}$ ) and  $\epsilon$  is the dielectric constant.

The relative magnetic permeability is given by [Ref. 1].

$$\mu_r = \frac{\mu}{\mu_0}, \quad (3.11)$$

where  $\mu$  is the magnetic permeability of earth and  $\mu_0$  is that of free space. As mentioned in Section C, the reflection coefficient of a plane smooth surface can be calculated by Fresnel's equations [Ref. 2,3]:

$$\Gamma_H = \frac{\sin \alpha' - (\epsilon_{rc} - \cos^2 \alpha')^{1/2}}{\sin \alpha + (\epsilon_{rc} - \cos^2 \alpha')^{1/2}} = \rho_H e^{-j\phi_H}, \quad (3.12)$$

$$\Gamma_V = \frac{\epsilon_{rc} \sin \alpha' - (\epsilon_{rc} - \cos^2 \alpha')^{1/2}}{\epsilon_{rc} \sin \alpha + (\epsilon_{rc} - \cos^2 \alpha')^{1/2}} = \rho_V e^{-j\phi_V}, \quad (3.13)$$

where  $\alpha'$  denotes the incident and reflected angle from a tilted surface (see Figure 3.3), and  $\phi_H$  and  $\phi_V$  are the horizontal and vertical phase of the reflected wave. The magnitude and phase of the reflection coefficient depends on the polarization, frequency and angle of incidence of the electromagnetic wave; and on the dielectric constant and conductivity of the surface.

The Fresnel Equations 3.12 and 3.13 correspond to two polarizations of the electric field. The subscripts  $H$  and  $V$  stand for horizontal and vertical polarizations respectively. Fresnel equations are given under the assumption that the wave is propagating in free space, and that the dielectric surface is non-magnetic.

When  $\alpha$  is equal to  $\frac{\pi}{2}$  (normal incidence), the horizontal and vertical reflection coefficients are identical in magnitude but opposite in sign. In this case Equations 3.12 and 3.13 become:

$$\Gamma_H = \frac{1 - \epsilon_{rc}^{1/2}}{1 + \epsilon_{rc}^{1/2}}, \quad (3.14)$$

$$\Gamma_V = \frac{\epsilon_{rc} - \epsilon_{rc}^{1/2}}{\epsilon_{rc} + \epsilon_{rc}^{1/2}} = -\Gamma_H. \quad (3.15)$$

### E. ILLUSTRATIONS OF REFLECTION COEFFICIENT OF A SMOOTH SURFACE

Figures 3.4 to 3.7 illustrate the dependence of the magnitude,  $\rho$ , and the phase,  $\phi$ ; on the grazing angle  $\theta$ , wavelength  $\lambda$ , and the polarization. In the case of vertical polarization there is a sharp decrease in the reflection coefficient due to the increase of transmission into the surface when the angle of incidence is close to Brewster angle, ( $\alpha_B$ ). At this angle  $\rho_V$  reaches its minimum. The phase  $\phi_V$  is [Ref. 2,3]:

$$\phi_V = \frac{\pi}{2} - \alpha_B. \quad (3.16)$$

In Figure 3.6 it is shown that  $\phi_V$  depends also on the wavelength of electromagnetic wave.

When the electric field is horizontally polarized, only slight variations occur in the magnitude and phase of the reflection coefficient ( $\rho_H$  and  $\phi_H$  respectively), with respect to the incidence angle (See Figures 3.4 and 3.5). The phase  $\phi_H$  is almost  $180^\circ$  for long wavelengths and increases slightly with incidence angle. In many practical applications  $\rho_H$  and  $\phi_H$  are approximately unity and  $180$  degrees ( $\pi$  radians) respectively, i.e.,  $\Gamma = -1$ . [Ref. 1,2]

For very small incident angles  $\rho_V$  and  $\phi_V$  are also close to unity and  $\pi$ , respectively. Such a case occurs for anti-ship sea-skimming missiles guided by a radar and for microwave searching radars operating close to the ocean surface. For incidence angles larger than  $10^\circ$ ,  $\phi_V$  decays to zero (see Figure 3.5). The characteristics mentioned

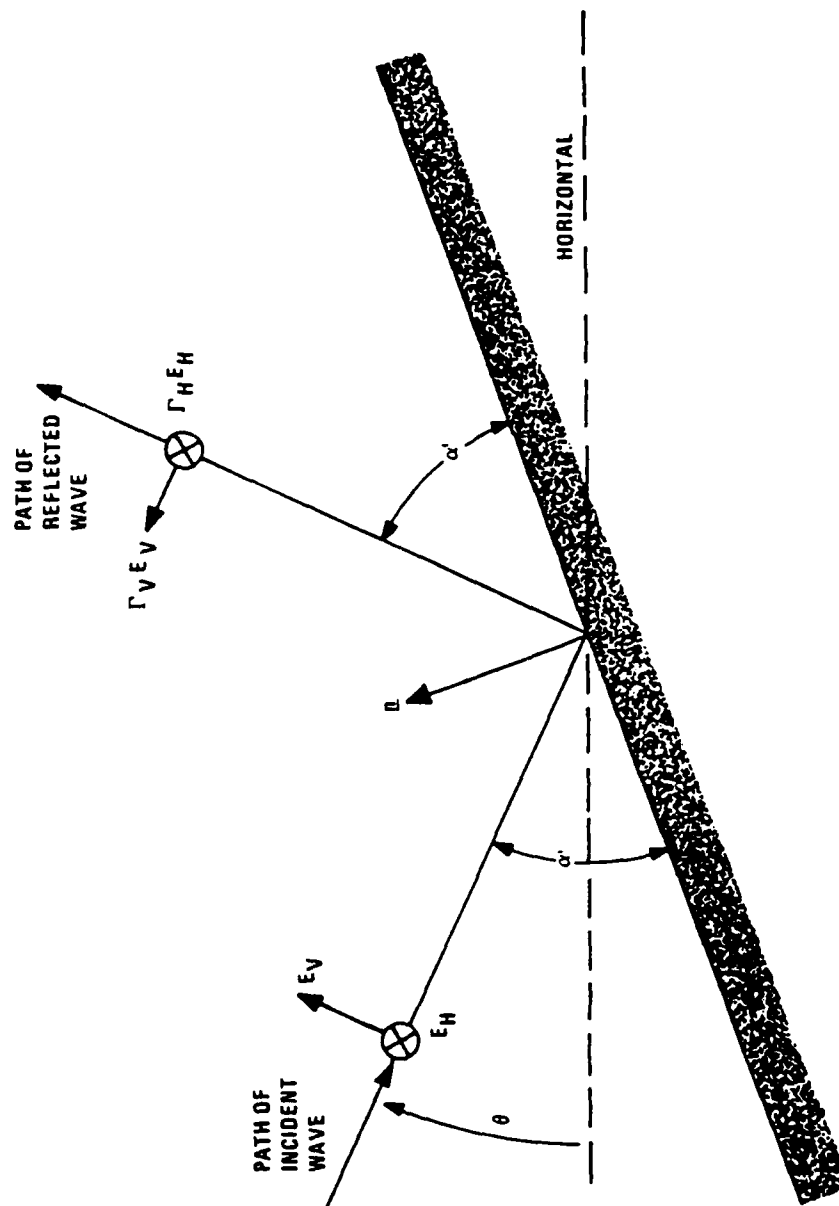


**Figure 3.3: Incident and Reflected Wave by a Smooth Dielectric Surface**  
 [From Ref. 2].

above for small incidence or grazing angles ( $< 1^\circ$ ) will play a major role also when the surface of incidence is rough. A complex effect of shadowing arises for small incidence angles and rough surfaces. This effect will be discussed in the next section.

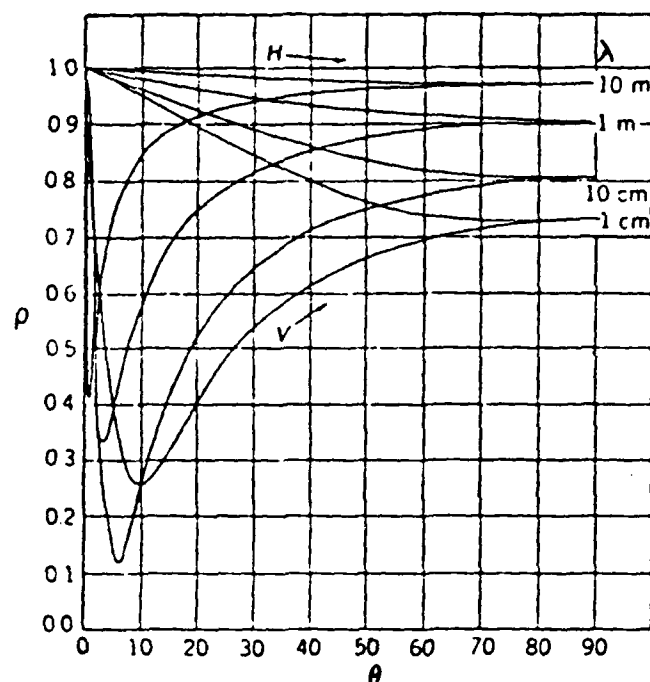


Figure 3.4: Reflection Coefficient of Very Smooth Sea Water [Ref. 2].

#### F. THE EFFECT OF SURFACE ROUGHNESS ON THE REFLECTION OF ELECTROMAGNETIC WAVES

In Chapter II we discussed the Rayleigh criterion and Fresnel zones for smooth surface approximation. In this section we will try to consider some more aspects of distinguishing between a rough and a smooth surface. Using Equation 2.4 for Rayleigh's criterion of smooth surface we get [Ref. 2,3]:

$$\frac{\Delta h \sin \theta}{\lambda} < \frac{1}{8}. \quad (3.17)$$

From this simplified criterion one would expect the reflection coefficient to be a function of wavelength, surface roughness, and grazing angle. This criterion gives only

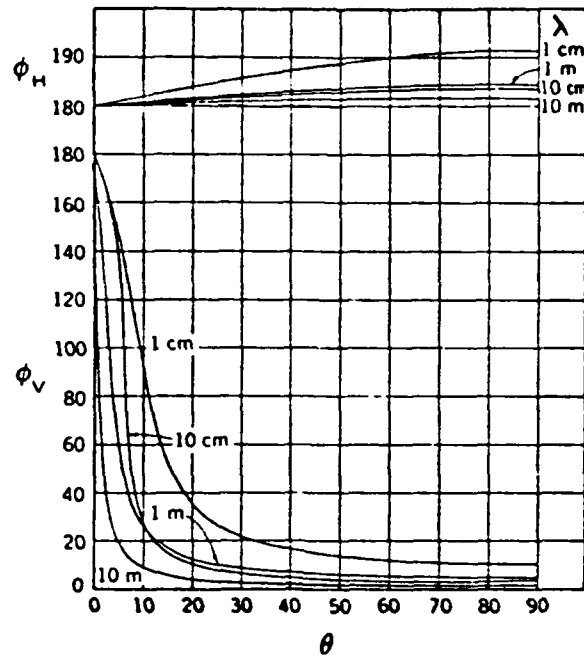


Figure 3.5: Phase of Reflection Coefficient  $\phi$  of Very Smooth Sea [Ref. 2].

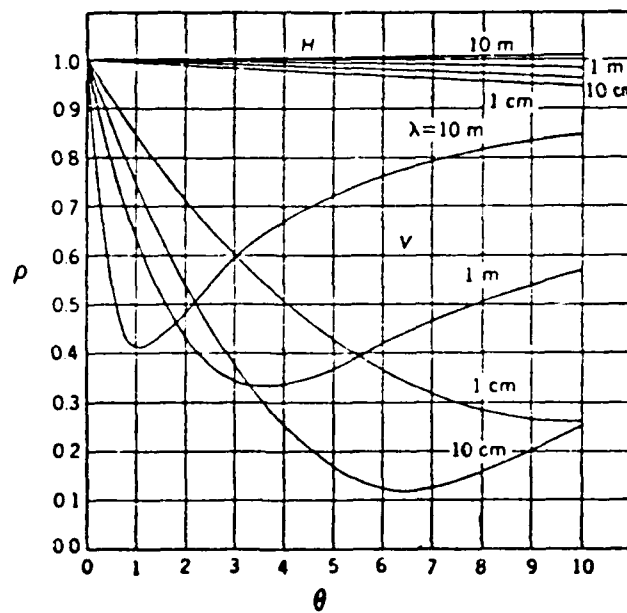
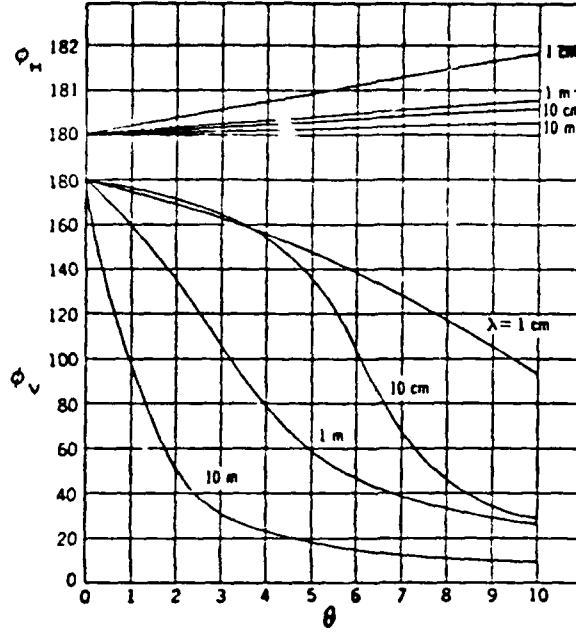


Figure 3.6: Reflection Coefficient for Low Depression Angles of Very Smooth Sea [Ref. 2].



**Figure 3.7: Phase of Reflection Coefficient for Low Depression Angle of Very Smooth Sea [Ref. 2].**

an approximate indication, dealing only with orders of magnitude. From empirical data it had been indicated that for large values of the parameter in Equation 3.17, where:

$$\frac{\Delta h \sin \theta}{\lambda} \gg \frac{1}{8}, \quad (3.18)$$

the reflection coefficient is independent of the parameter  $\frac{\Delta h \sin \theta}{\lambda}$  for a specific surface. However, small values of  $\frac{\Delta h \sin \theta}{\lambda}$ , the reflection coefficient increases with an increase of the parameter. Actually there is no sharp distinction between rough and smooth surface. [Ref. 4]

One fundamental result from analyzing the scattering field from a rough surface is that it consists of two components, a coherent or specular component and an incoherent or diffused component. [Ref. 1]

The **specular reflection** is defined as a single reflection of electromagnetic wave from a rough surface in the direction of the receiver. Its reflection obeys the optical laws and its phase is coherent. In other words, the reflected waves from a rough surface



can be considered as specular if they arrive at the receiver with equal phases and have relatively small amplitude fluctuations. These reflections are from the Fresnel zones as described in Chapter II.

The diffused scattering is scattered randomly from a much larger area than the first Fresnel zone. Its phase is uniformly distributed, but the large fluctuations of its amplitude are Rayleigh distributed. [Ref. 1]

These two components were observed in several experiments. The specular reflected field, when combined with the direct field, will produce at a test receiver a periodically varying field. When a diffuse field is added to the direct field, the result will be a randomly varying field. [Ref. 1,3]

Specular reflection and diffuse scattering often occur simultaneously. The diffused scattered field could be the reflection from large numbers of uncorrelated scatterers. It would be expected that the reflection is totally diffused and independent of phase difference  $\Delta\phi$ . This is not always true, since in the case of perfectly smooth surfaces the diffused field is zero [Ref.4]. Also the specular field may be produced by many scatterers since it can be produced by a linear summation of many specular fields. In reality, the total field is the sum of both the specular and diffused fields.

Many attempts were made to model a reliable specular reflection coefficient, caused by a Gaussian distributed surface as a function of mean wave height of the sea, grazing or incident angle  $\theta$ , and the transmitting wavelength  $\lambda$ . The improved reflection coefficient  $\rho_s$  does not take into account the shadowing effect. The magnitude of the specular reflection coefficient is calculated by [Ref. 2]:

$$\rho_s = \rho_0 \cdot D R_s, \quad (3.19)$$

where  $R_s$  is the specular scattering coefficient for rough surface,  $\rho_0$  is the reflection coefficient of a plane and perfectly smooth surface, and  $D$  is the divergence coefficient due to earth's curvature. Modifications in the reflection coefficient caused by a Gaussian distributed rough surface was calculated by Beckman [Ref. 1]. The mean square

variations in  $R_s$  is given by:

$$\langle R_s^2 \rangle = e^{-2(\Delta\phi)^2}. \quad (3.20)$$

The phase difference  $\Delta\phi$  is calculated by:

$$\Delta\phi = 2\pi\Delta h \sin \theta / \lambda, \quad (3.21)$$

where  $\Delta h$  represents the standard deviation of the Gaussian distribution of wave heights [Ref. 2]. Equation 3.21 is an analogy of phase difference for Rayleigh criterion (Equations 2.2, 2.4). The improvement in Equation 3.21 is that  $\Delta h$  is not just a magnitude but defined more correctly.

Most of the properties of reflection from a smooth surface can be applied to specular reflection from a rough surface. The basic difference is that specular reflection [Ref. 1]:

- 1) fluctuates, and,
- 2) is smaller in amplitude.

These facts are taken into account through the specular scattering coefficient  $R_s$ .

Different models for  $\langle R_s^2 \rangle$  were suggested. In all of these  $\langle R_s^2 \rangle$  is a function of the phase difference  $\Delta\phi$ . The additional models of  $\langle R_s^2 \rangle$  are [Ref. 1]:

- 1) a uniformly distributed surface:

$$\langle R_s^2 \rangle = \text{sinc}^2 \Delta\phi, \quad (3.22)$$

- 2) first Fresnel zone of a uniformly distributed surface:

$$\langle R_s^2 \rangle = (1 - \Delta\phi/\pi) \text{sinc}^2 \Delta\phi. \quad (3.23)$$

By checking these three models (Equations 3.20, 3.22, 3.23) against experimental results, the improved Gaussian surface distribution, Equation 3.20, gave the closest results to the experimental ones [Ref. 2]. Figure 3.8 illustrates the dependence of the mean square of the reflection coefficient, on the phase variance, for the improved Gaussian model.

From experiments it was seen that there were some variations of  $\langle R_s^2 \rangle$  from the curve when the abscissa is  $> 120$  mradians. Those variations were caused, probably, by diffused scattering; or by the combination of diffused and specular, scattering/reflection [Ref. 2].

Until now we have discussed, quantitatively, only the specular reflection from a rough surface. Now we want to define and analyze the diffused scattering. The reflection coefficient of diffuse scattering  $\rho_d$  can be written similarly to the specular reflection coefficient:

$$\rho_d = \rho_0 D R_d, \quad (3.24)$$

where  $R_d$  is the coefficient which defines the irregularities of the surface, and  $\rho_0$  is the reflection coefficient of a smooth surface. The amount of power in the diffused field may also be a function of polarization. The values of  $R_d$  that were measured in experiments is within the range of 0.2–0.4, while the mean values were between 0.3–0.35. When  $\theta = 0$  (grazing incidence),  $\Delta\phi = 0$ , according to Equation 3.21; and  $\langle R_s^2 \rangle = 1$ . Under these conditions,  $\rho_s = D\rho_0$ . This means that the specular (coherent) component is equal to the value of the field for a smooth surface. As  $\theta$  increases, the diffuse (incoherent) component increases, until the phase difference approaches the value of 120 mradians. From this point the diffused component decreases. Also, an increase in  $\theta$  decreases the specular component (see Equations 3.19–3.21). [Ref. 2,4]

For sea surface, one of the models for forward scattering expresses the electric scattered field as a vectorial summation of the specular and diffused fields with zero mean. The phase of the specular field is equal to the phase for a smooth sea; its magnitude is reduced by the scattering coefficient (Equation 3.19). [Ref 3]

Measurements were made by Beard [Ref. 12] on the reflected field above sea surface, for roughness varying from smooth sea  $\frac{\Delta h \sin \theta}{\lambda} < \frac{1}{8}$  till the value of  $\frac{\Delta h \sin \theta}{\lambda} = \frac{1}{3}$ . The transmitting wavelengths were 0.86, 4.2, and 5.3 cm. Both polarizations, vertical and horizontal, were introduced separately. The measured results indicated that [Ref. 2]:

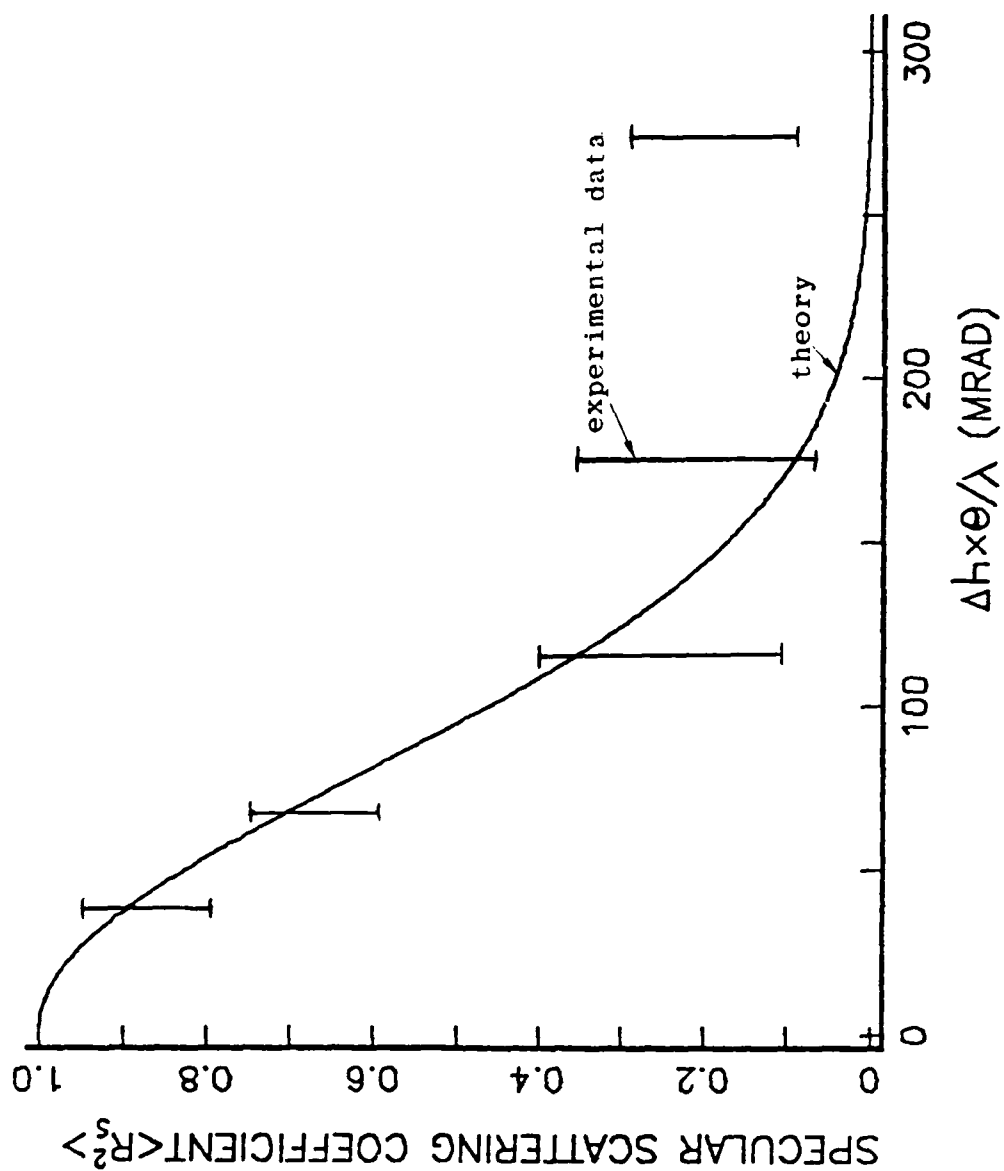


Figure 3.8: Dependence of Mean Square of Scattering Coefficient on Phase Variance, for Specular Reflection from Rough Surface [Ref. 2].

- 1) The maximum values of power contained in the diffused field is approximately 30% of the specular reflection.
- 2) For both polarizations, the results did not change the polarization independence.

Probably the most common distribution of forward scattered field from a sea surface is the Ricean distribution; which is a result of a model where the amplitude fluctuation of the forward scattered diffused field is Rayleigh distributed, and its phase is uniformly distributed. This model has proven to be a good approximation, also, by experimental results. It should be noted that for very low grazing angles, the ratio of the diffused to specular powers is 2-3 time larger than for higher incidence or grazing angle. [Ref. 3,6]

The root mean square (RMS) of the sea wave height  $\Delta h$  can be deduced by observation or from sea state tables. These values are given in Table 3.1, and will be used in Chapter IV to calculate the coverage pattern of the radar due to multipath.

**TABLE 3.1: PARAMETERS OF SEA STATE. [REF. 1,7].**

Sea State	Type of Roughness	Wave Height [m]	RMS Height [cm]
0	calm	0	0
1	smooth	0-0.3	0-6.5
2	slight	0.3-1	6.5-21
3	moderate	1-1.5	21-32
4	rough	1.5-2.5	32-54
5	very rough	2.4-4	54-86
6	high	4-6	0.86-1.3

## G. SHADOWING EFFECT

When radar operates at very low grazing angle ( $< 1^\circ$ ), the scattering from the surface will be "partial". This means that large parts of the electromagnetic wave lie in

the geometric shadow of the sea wave crest [Ref. 3]. The trough of the wave is not seen directly, though some of the shadowed areas are seen due to refraction illumination.

However, for grazing angles less than  $1^\circ$  the shadow effect greatly affects the backscatter echo.

Two analytical approaches were developed for the shadowing problem. A statistical exercise in geometrical optics and a diffraction problem in which geometrical optics shadowing theory is considered. The procedure of the statistical approach involves many statistical expressions, but eventually results in a shadowing function which is the percentage of the illuminated surface area at a specific grazing angle. At small angles it is a linear function of the angle. This approach has not yet been proven as representing reliable practical shadowing effects at low grazing angles. [Ref. 6]

In the geometrical shadowing theory mentioned above, it was found that at extremely low grazing angles ( $< 1^\circ$ ) the sea surface resembles a dark plane with illuminated "spots". The size and location of these spots, within the reflecting plane, are a function of the wind speed and the grazing angle. This result is closer to the practical radar picture, involving such phenomenon as sea spikes, rather than the shadowing function picture which presents diffuse, vanishing, scatter. However, this geometrical theory should be checked carefully before applying it to practical cases. [Ref. 2,6]

## H. DEPOLARIZATION

Depolarization is defined as a change in the polarization of an electromagnetic wave due to propagation (in a medium other than free space) and including surface diffraction, reflection, and scattering.

In describing quantitatively the depolarization scattered from an object, a so-called scattering matrix is derived. The scattering matrix describes completely the phase and amplitude of the reflected electromagnetic wave at the receiver. For better understanding, suppose that an electromagnetic plane wave is transmitted with its electric field in the  $y$  direction (see Fig 3.9), and represented by  $E_y^i$ . Let the reflected

field from an object (or a surface) at the receiver, be represented by  $E_x^r$ , and be given by [Ref. 8]:

$$E_x^r = \rho_{yx} E_y^i, \quad (3.25)$$

where  $\rho_{yx}$  represents the reflection coefficient of the incident surface and/or object. (The first subscript stands for the transmitted field and the second subscript stands for the receiving component.) The reflection coefficient  $\rho_{yx}$  is complex, and includes the change in phase and amplitude, of the incident field.

Since any polarization of a plane wave can be described by two orthogonal components, polarized linearly, a scattering process can be described completely by the polarization scattering matrix [after Ref. 8]:

$$\begin{bmatrix} E_x^r \\ E_y^r \end{bmatrix} = \begin{bmatrix} \rho_{xx} & \rho_{yx} \\ \rho_{xy} & \rho_{yy} \end{bmatrix} \begin{bmatrix} E_x^i \\ E_y^i \end{bmatrix}. \quad (3.26)$$

Figure 3.9 illustrates two linear and orthogonal electric fields, which produce by summation a right circular electric field. For a perfect conducting plane surface,  $\rho_{xx}$  should be equal to  $\rho_{yy}$ . Also, the scattered energy (square electric field) from a surface is mainly a function of the transmitted wavelength and the reflecting surface orientation and roughness. [Ref. 8]

In 1963 it was shown by Beckman and Spizzichino [Ref. 1] that, if a plane wave is purely polarized (horizontally or vertically), no depolarization will occur in the reflected wave in the plane of incidence. If the same incident wave will be scattered out of the incident plane, it will be strongly depolarized. These scattered components are a result of the irregularities of the incident surface, and related to the diffused scattering. [Ref. 1]

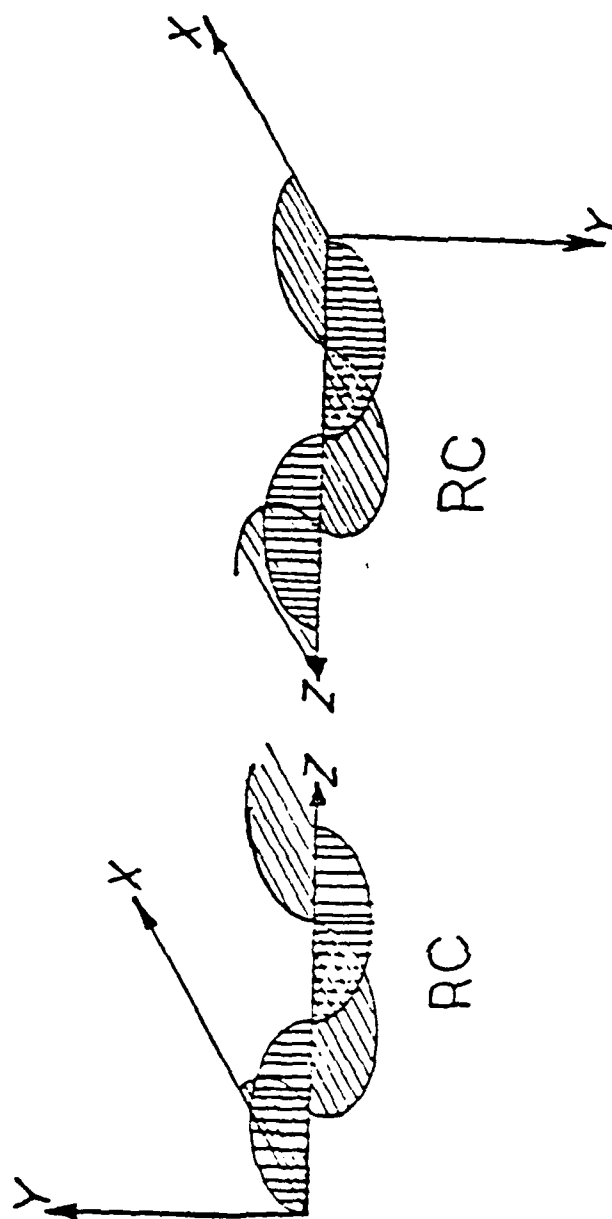


**Figure 3.9: Right Circular Polarization Produced by Horizontal and Vertical Polarizations [Ref. 8].**



According to experiments above sea surface, with near purely polarized wave, the received depolarized specular component is very small (at least 25 dB below the incident polarization). On the other hand, the diffused scattered field is strongly depolarized.

From these results one can conclude that for forward scattering from sea surface, depolarization, for linear polarization is small. This fact can also be verified when looking at echoes reflected from targets, especially on a smooth sea. These echoes might fluctuate sharply due to interference of the direct and the reflected wave. The interference can occur only if the reflected field has largely the same polarization and magnitude as to the direct field. It is shown in Ref. 1 that very little depolarization takes place in the direction of specular rays. Therefore the interference effect is additional evidence that depolarization, due to reflection from sea surface is small [Ref. 2]. This phenomena will be discussed and analyzed in Chapter IV.

## **IV. LOBING PHENOMENA ANALYSIS**

### **A. INTRODUCTION**

In Chapters II and III we have described the characteristics of earth's surface and a little about air refraction (for more detail see Chapter V), which dramatically affects electromagnetic propagation.

In this chapter we will discuss and analyze the influence of these characteristics on a Naval search radar (shipborne, shore installation and low-flying aircraft).

We can assume that the detection range of a very low altitude target will be limited due to multipath propagation and earth's curvature [Ref. 11].

In this chapter we will discuss and analyze the lobing phenomena, caused by multipath, based on the parameters described in Chapter II and III. We will consider specifically the sea surface, and the detection conditions of a Naval search radar, which usually views the sea at extremely low grazing angles ( $< 1^\circ$ ). The covering pattern of detection for these radars is strongly affected by the multipath of the propagating electromagnetic wave. The multipath causes constructive and destructive interference due to earth reflection. This effect, together with media and radar parameters, will be computed to illustrate predicted detection patterns of the radar.

We will complete the analysis with some practical conclusions and recommendations for some control on the pattern coverage for a Naval radar.

### **B. MULTIPATH FADING PHENOMENA**

The main sources of multipath fading are reflections from the earth's surface and from refracting layers in the atmosphere. In the commonly known multipath, there are

two such paths—a direct path of the transmitting wave from the radar to the target and an indirect path from the radar to the target via reflection.

The geometry of this scenario is shown in Figure 3.1. From this figure it is seen that the direct and indirect wave have traveled different paths. If these waves have the same order of magnitude they can strongly interfere. They will have phase differences caused by path differences. A quantitative analysis of the lobing phenomena was done by Blake and is described herein [after Ref. 9].

Destructive interference will occur when the absolute value of the phase difference is between  $\frac{\pi}{2} + 2\pi n$  and  $\frac{3\pi}{2} + 2\pi n$  radians ( $n$  is integer). When the phase difference is  $\pi$  radians ( $180^\circ$ ) and the amplitudes of the direct and indirect field are almost the same, a complete cancellation will occur at the receiving point. Constructive interference will occur if the absolute value of the phase difference is between  $0 + 2\pi n$  and  $\pi/2 + 2\pi n$ . When there is no phase difference ( $\phi = 0$ ), the constructive interference will be of maximum value due to arithmetic summation of the amplitudes.

This phenomena can be seen, if we look at the field at a fixed height, as a function of the range. We will cross through maxima and minima of the field pattern of the radar, caused by interference.

The goal of this discussion will be to derive procedures and equations in order to predict radar range performance under multipath conditions. We will derive the lobing factor  $F$ ; considering the flatness of the earth, sea roughness and polarization. This was discussed in Chapters II and III. For simplification, we will assume that the target is far enough so that the usual far-field approximations are valid.

## C. THE LOBING FACTOR

The analytical treatment of the interference phenomena has to be in the complex plane, since we are dealing with amplitudes and phases of the waves. Basically, the phase difference of the direct and reflected wave is dominated by three factors:

- 1) the geometric path length difference  $\delta$  (see Equations 2.6, 2.7),
- 2) the phase difference of the reflected wave due to the reflection process, and,
- 3) phase difference due to radiation of the antenna in direct and indirect directions.

The amplitude difference can be caused by the following reasons:

- 1) The Naval radar with narrow beam in the horizontal plane is usually not uniform in the vertical plane which can cause different field intensities in the direct and indirect waves.
- 2) Both waves propagate spherically, resulting in an inverse square law power reduction. Since the path of the waves is different they will be attenuated or spread differently.
- 3) The reflected wave is usually attenuated because the sea surface reflection coefficient is less than unity.

### 1. Applications

The spreading loss is usually neglected for both waves due to the small path difference  $\delta$  between the direct and reflected wave. The major effect of  $\delta$  is on the phase difference. Most of the Naval surface surveillance radars are pulsed radars. The effect of interference can occur only if  $\delta < c\tau$ , where  $\tau$  is the pulse width and  $c$  is the speed of light in free space. For surface and low flying targets and moderate height of radar antennas,  $\delta \ll c\tau$  [Ref. 5,9]. This will result in susceptibility to the multipath effect. For radars which use pulse compression techniques the criterion of  $\delta < c\tau$  is for the compressed pulse.

### 2. Combined Phase Difference $\alpha$ , and Detecting Range $R_d$

The magnitudes of the reflection coefficient  $\rho$ , and the pattern factor of the antennas  $f(\gamma)$ , are major effects on the amplitude of the reflecting wave. The elevation

angle between the radar antenna and the target/receiver is  $\gamma$  (see Figure 4.1). The ratio of the electric intensity in the direction of the reflected ray to the intensity of the maximum beam direction (boresight) is  $f(\gamma_r)$ , while  $f(\gamma_d)$  is the same ratio in the direction of the direct ray. Both  $|f(\gamma)|$  and  $\rho$  are bounded in the range of 0 and 1.

Now we can derive a phasor expression for the direct and indirect wave fields. The direct wave field can be written as:

$$E_d = f(\gamma_d)E_0, \quad (4.1)$$

where  $E_0$  is the phasor value of the free space field in the beam maximum at the target range  $R_d$ . Similarly, the reflected wave field is:

$$E_r = f(\gamma_r)E_0 \cdot \rho e^{-j\alpha}, \quad (4.2)$$

where  $\alpha$  is the total phase difference caused by three factors mentioned in Section C of this chapter, and  $\rho$  is the magnitude of the reflection coefficient. The combined field at the target is:

$$E = E_r + E_d, \quad (4.3)$$

Substituting Equations 4.1 and 4.2 into 4.3 yields:

$$E = E_0 [f(\gamma_d) + f(\gamma_r)\rho e^{-j\alpha}], \quad (4.4)$$

the lobing factor  $F$  is defined as:

$$F = |E/E_0|. \quad (4.5)$$

Dividing Equation 4.5 by  $E_0$  yields:

$$F = |f(\gamma_d) + \rho f(\gamma_r)e^{-j\alpha}|. \quad (4.6)$$

If we assume that  $\alpha$  includes the phase difference  $\beta_r - \beta_d$  of the pattern factor, then by factoring out  $f_d$  and using Euler's theorem, the lobing factor  $F$  is written as:

$$F = f_d \left| \sqrt{1 + x^2 + 2x \cos \alpha} \right|, \quad (4.7)$$

where

$$x = \frac{\rho f_r}{f_d}, \quad (4.8)$$

$f_r$  and  $f_d$  are scalar magnitudes of the direct and reflected pattern factors.

We can represent the pattern factor  $f(\gamma_d)$  and  $f(\gamma_r)$  in the form of:

$$f(\gamma_d) = f_d e^{-j\beta_d}, \quad (4.9)$$

$$f(\gamma_r) = f_r e^{-j\beta_r}, \quad (4.10)$$

where  $\beta_d$  and  $\beta_r$  are phase angles and  $f_d$  and  $f_r$  are the magnitudes of the pattern factors.

As mentioned,  $\alpha$  is the total phase difference between the direct and reflected waves and can be expressed as:

$$\alpha = \frac{\pi\delta}{\lambda} + \phi + \beta_r - \beta_d, \quad (4.11)$$

where the first term in  $\alpha$  is caused by path difference, the second term ( $\phi$ ) is caused by the reflection process, and the third term ( $\beta_r - \beta_d$ ) is the phase difference of the pattern factors.

The detection range in presence of multipath and atmospheric loss  $L$  can be calculated by:

$$R = \frac{R_0 F}{L^{1/4}}, \quad (4.12)$$

where  $R_0$  is the free space detection range. For analyzing the lobing effect we will propose that no atmospheric loss occurs, and Equation 4.8 is simplified to:

$$R = F R_0. \quad (4.13)$$

Equation 4.13 is a realistic approximation for radar frequencies, since the lobing factor is dominant when multipath occurs and affects the detection range more than the atmospheric losses. Since  $0 \leq F \leq 2$ , it is seen that the range  $R_d$  under multipath conditions is sometimes greater than the free space range, and sometimes smaller than the free space range.

#### D. PATH DIFFERENCE DERIVATION

The actual antenna pattern located at  $A$  in Figure 4.1 can be found by treating it as a two source interferometer caused by the real antenna and its image from the ground at  $C$  [Ref. 5]. The range  $R_d$  is the flat earth approximation range. If we assume that  $R_d \gg h'_1$  then the difference between the direct path  $AE$  and the indirect path  $ADE$  is:

$$\delta = 2h'_1 \sin \theta, \quad (4.14)$$

Recall from Chapter III, Section A,  $h'_1$  is the height of the radar antenna and  $\theta$  is the incident (grazing) and reflected angle of the indirect ray.

For small grazing angles, which are typical of sea surface search radars,  $\sin \theta$  can be expressed as:

$$\sin \theta = \frac{h'_1 + h'_2}{R_d}, \quad (4.15)$$

where  $h'_1$  is the height of the target. By assuming that  $h'_2 \gg h'_1$  and knowing that  $R_d \gg h'_1$  the further approximation can be made:

$$\sin \theta \approx \frac{h'_2}{R_d}. \quad (4.16)$$

By substituting Equation 4.16 into 4.14, the path difference can be approximated by:

$$\delta \approx \frac{2h'_1 \cdot h'_2}{R_d}, \quad (4.17)$$

By multiplying Equation 4.17 with the wave number,  $k = \frac{2\pi}{\lambda}$ ; the result is the approximate but practical phase difference  $\Delta\phi$ , for a plane reflecting surface:

$$\Delta\phi \approx \frac{2\pi}{\lambda} \cdot \frac{2h'_1 \cdot h'_2}{R_d}. \quad (4.18)$$

The elevation angle  $\gamma_d$ , and the depression angle  $\gamma_r$ , can be calculated by geometric considerations:

$$\gamma_d = \sin^{-1} \frac{h'_2 - h'_1}{R_d}, \quad (4.19)$$

and

$$\gamma_r = \sin^{-1} \frac{h'_2 + h'_1}{R_1 + R_2}. \quad (4.20)$$

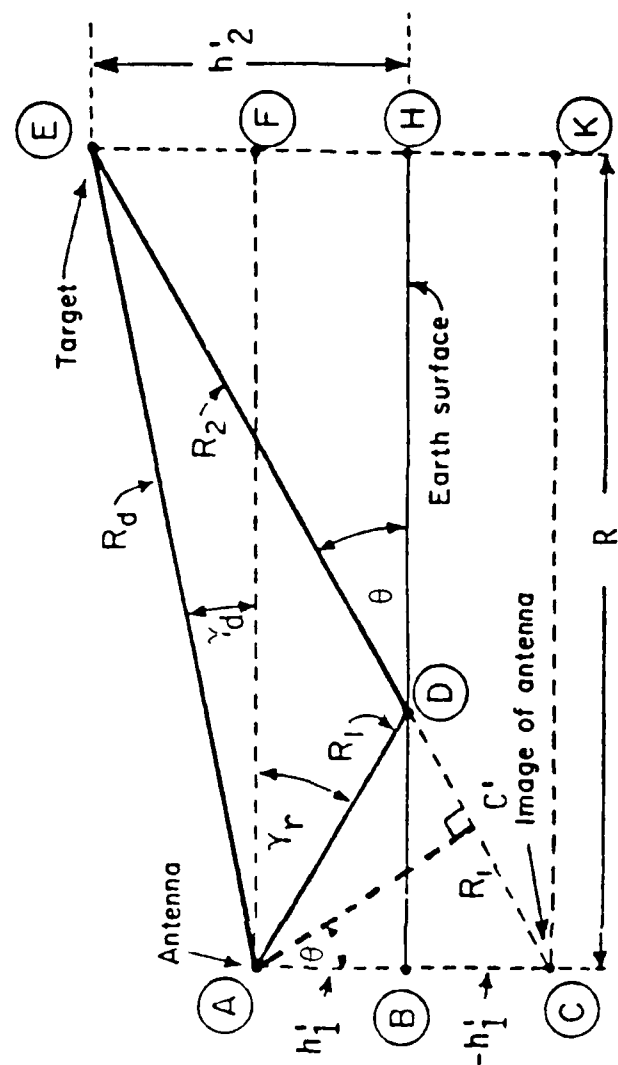


Figure 4.1: Multipath Geometry over a Plane Reflecting Surface [Ref. 9].



Again by using the assumptions  $h'_2 \gg h'_1$  and  $R_d \gg h'_1$  we conclude that :

$$\gamma_d = \gamma_r = \theta. \quad (4.21)$$

By using the identity of Equation 4.21 in Equation 4.14 there results:

$$\delta = 2h'_1 \sin(\gamma_d). \quad (4.22)$$

This geometric solution of the multipath effect is not complete since we have to consider also the reflection coefficient which is a function of the grazing angle  $\theta$ .

### E. PRACTICAL LOBE FACTOR DERIVATION

The solution for the lobing factor is achieved by substituting Equation 4.17 into Equation 4.11; this result for  $\alpha$  is substituted into Equation 4.7 together with the magnitudes of the pattern factors and the reflection coefficient. [Ref. 3,9]

A special, practical, and simplified result is obtained for a perfectly smooth sea and horizontal polarization. For this case, Figures 3.6 and 3.7 indicate that  $\rho \simeq 1$ , and  $\phi \simeq \pi$  rad, independent of grazing angle.

For surface search and navigation radars the main beam is narrow and directed at zero elevation angle, and the vertical beam is broad. Under these conditions  $\beta_d = \beta_r$  and  $f_d = f_r = 1$  and

$$\alpha = \frac{2\pi\delta}{\lambda} + \pi. \quad (4.23)$$

Substituting this simplification into Equation 4.7 yields:

$$F = \left| \sqrt{2 + 2 \cos(2\pi\delta/\lambda + \pi)} \right|. \quad (4.24)$$

By trigonometric manipulation:

$$F = 2 \left| \sin(\pi\delta/\lambda) \right|. \quad (4.25)$$

By substituting Equation 4.21 into 4.24 we obtain, finally, an especially useful result for the lobing factor,  $F$ :

$$F = 2 \left| \sin \left[ (2\pi h'_1 \sin \gamma_d) / \lambda \right] \right|. \quad (4.26)$$

## F. DISCUSSION

Equation 4.26 allows us to predict the relative lobing pattern without knowing the range and altitude of the target. The lobing factor  $F$  depends only on the elevation angle  $\gamma_d$ . Figure 4.2 is a plot of the lobing factor  $F$  showing the vertical plane coverage affected by typical multipath from a smooth sea. The antenna height is 10 meters and the transmitting frequency is 100 MHz.

Note that the maximum range  $R_d$  is twice the free space range  $R_0$  due to constructive interference since the maximum value of  $F$  is 2. On the other hand, when the target is located at other elevation angles than the maximum beam value, the detection range can be less than the maximum free space range. When the target is in the direction of nulls, no detection will occur.

As seen in Figure 4.1, variations of detection range relative to free space are bounded between the two extremes, 0 and 2, and are a function of the elevation angle. At a lobe maximum, we have [Ref. 5,9]:

$$\gamma_{\max}(n) = \sin^{-1} \frac{(2n+1) \cdot \lambda}{4h'_1} \quad n = 0, 1, 2, \dots \quad (4.27)$$

The minimum occurs when the same argument is equal to multiples of  $2\pi n$ . The elevation angles at which minima occurs is given by:

$$\gamma_{\min}(n) = \sin^{-1} \frac{n\lambda}{2h'_1} \quad n = 0, 1, 2, \dots \quad (4.28)$$

Equations 4.27 and 4.28 indicate that the maxima and minima angles depends only on the wavelength and antenna height. This is true only under the following assumptions [Ref. 9]:

- 1) The pattern factor phase difference  $\beta_d - \beta_r$  is constant at all elevation angles.
- 2) The phase of the reflection coefficient is also constant.
- 3) The reflecting surface is plane and not curved.

These assumptions are good approximations for horizontal polarization and an antenna pattern with zero elevation beam. If we take into account also the reflection

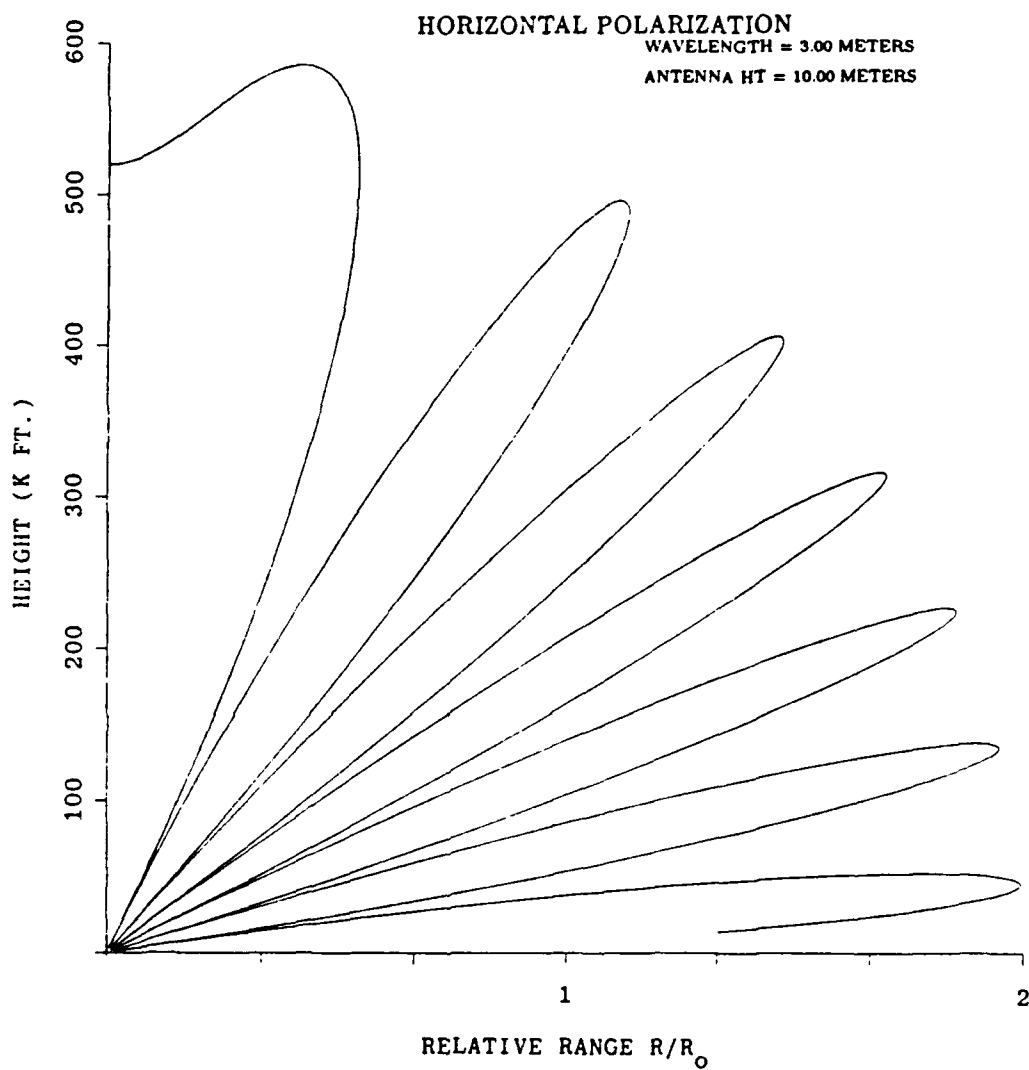


**Figure 4.2: Vertical Lobe Pattern Caused by a Plane Reflecting Surface.**

coefficient and antenna pattern factors, it affects the envelope of the covering factor, as we will see in Section G of this chapter.

The free space radar equation for the received signal should be modified by the lobing factor. Due to free space loss the received power  $P_r$  of a radar (two-way loss) is proportional to:

$$P_r \propto \frac{1}{R_0^4}. \quad (4.29)$$

Doubling the free space detection range  $R_0$  caused by constructive interference is equivalent to increase the transmitting power or the sensitivity of a radar 16 times or equivalently by 12 dB.

Equation 4.28 yields that the first minima occurs at zero elevation angle. This is not true for a curved surface in which the first minimum is not zero and its elevation angle is not zero. Near the horizon when the grazing angle approaches zero, the lobing factor is very low causing a very low field strength at this region. The returned signal is dominated by the spherical nature of the wavefront, resulting in scattering which can be taken into account by the divergence factor  $D$  [Ref. 3]. This is the reason why targets at very low grazing angles (low altitude), much under the first maximum lobe angle are difficult to detect. Typical targets with low grazing angles with respect to shipborne radars are anti-ship sea skimming missiles. This is the reason for the effort being made trying to predict and control the location and shape of the first interfering lobe.

The flat earth equations that were presented in this chapter are good approximations for relatively low antenna height such as shipborne searching radars where the reflecting point is close to the radar.

## G. LOBING ANALYSIS FOR TYPICAL CASES

We want to now analyze plots of detection patterns affected by multipath for radars operating above sea surface. In Figure 4.2 we saw a detection contour of a low frequency radar (100 MHz) with horizontal polarization and antenna height of 10 meters operating above a perfectly smooth surface. Figure 4.3 is the detection contour

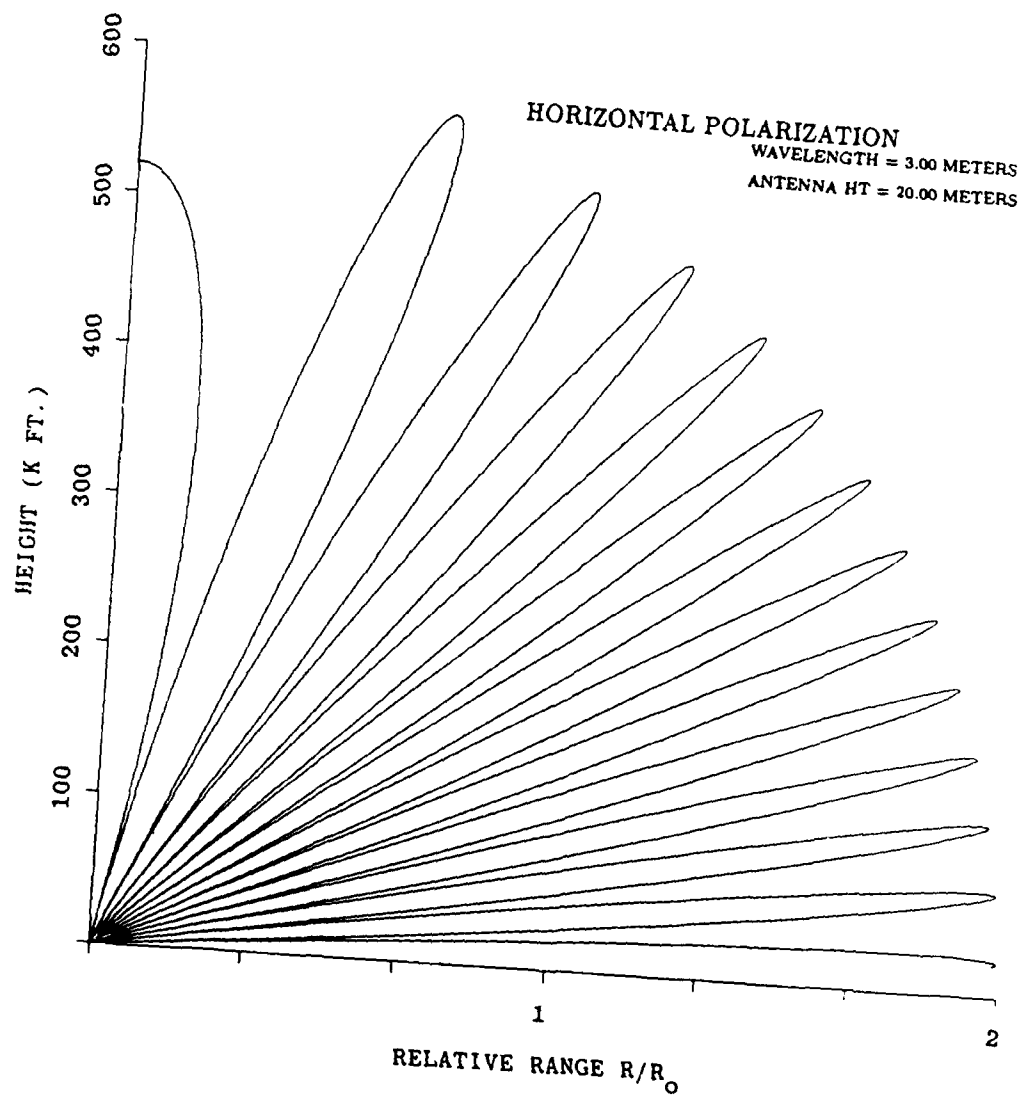
of the same radar except that the height of the antenna is doubled to 20 meters. This has an effect of lowering the angle of the first lobe and doubling the number of lobes nulls.

Figure 4.4 is a detection plot of a radar under the same conditions as Figure 4.3 except the frequency is now 10 times higher (1000 MHz). This effect also lowers the first beam and reduces considerably the uncovered space between the lobes. The number of lobes and nulls are increased by the ratio of frequencies (10 times). Also, according to conservation of energy, the lobes are 10 times narrower. One can conclude that the "penalty" for lowering the first lobe by increasing the antenna height and/or the frequency is that the number of nulls is increased proportionally (no received echo in null angles) and that the lobes are narrowed proportionally. For shipborne and shorebased surface search radars, increasing the frequency and the antenna height is recommended for improved detection of targets with low grazing angles like small surface combatants and low flying aircraft/missiles.

If the polarization of the transmitting wave is vertical, the covering pattern will be reduced. This is particularly true for the lower lobes, due to reduced values of the reflection coefficient  $\rho$ , at low angles (see Figure 3.4). Also, the phase difference is not  $180^\circ$  as it was in the case of horizontal polarization (see Figure 3.5), resulting in higher angles of maxima and minima. [Ref. 9]

In Figure 4.5 we include also the effect of the antenna pattern of a rectangular antenna with its electric field uniformly distributed. The pattern is derived from the Fourier transform of the rectangular uniform distribution resulting in a  $\frac{\sin x}{x}$  shape. By comparing with Figure 4.3, we see that this has the effect of modulating the basic pattern. Also the higher order lobes have a reduced coverage.

We now investigate the influence of the scattering coefficient  $R_s$ , considered in Chapter III, on the radar range. The effect of this parameter is to reduce the detection range progressively at higher grazing angles. This is because  $\langle R_s^2 \rangle$  decreases exponentially with increasing grazing/elevation angle  $\theta$ . Recall from Equations 3.20 and



**Figure 4.3: Vertical Lobe Pattern for the Same Parameters as Figure 4.2 Except Antenna Height Increased to 20 m.**

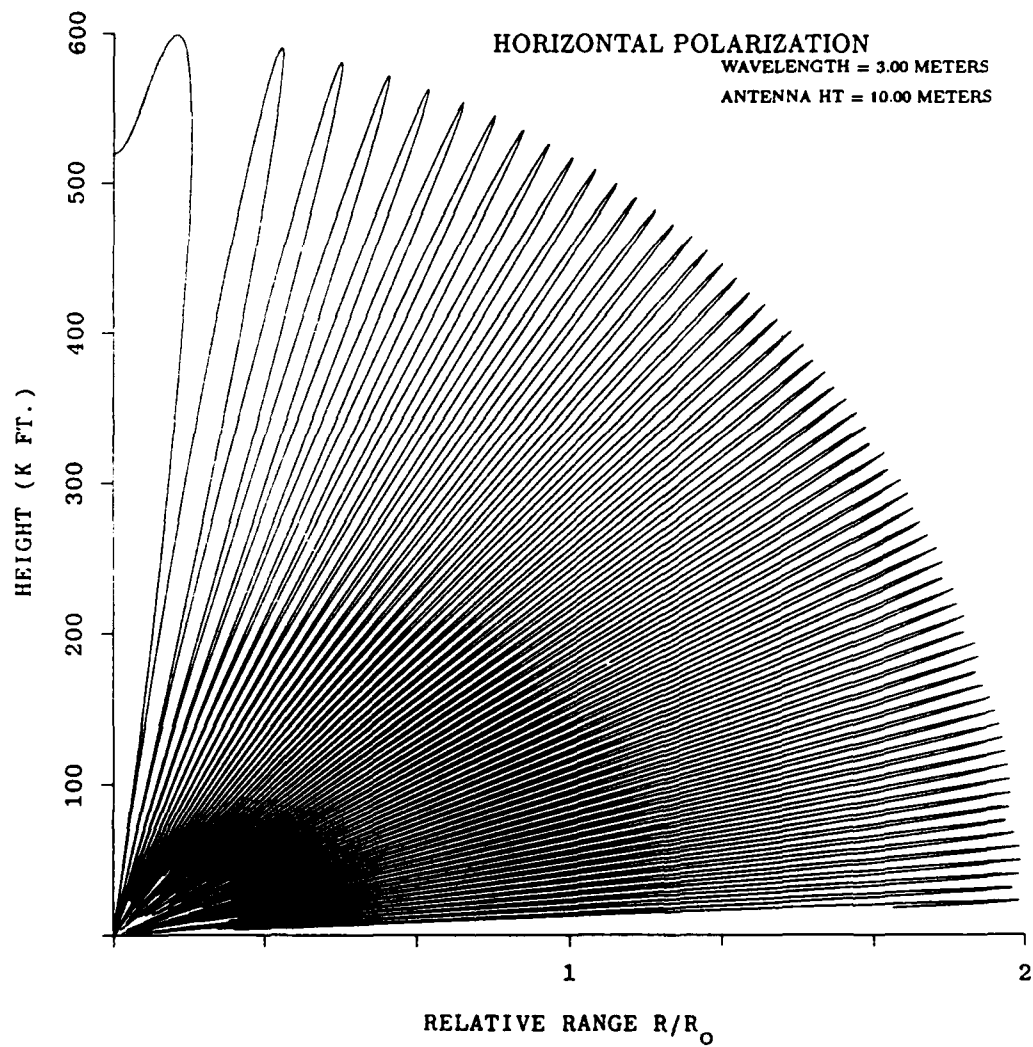


**Figure 4.4: Vertical Lobe Pattern for the Same Parameters as Figure 4.2 Except the Frequency is Ten Times Higher (1000 MHz).**

3.21 that the mean square variation in  $R_s$  is given by:

$$\langle R_s^2 \rangle = e^{-2(2\pi\Delta h \sin \theta / \lambda)^2}. \quad (4.30)$$

Figure 4.7 is a plot with same parameters as in Figure 4.6 but for a higher roughness of sea surface. By increasing the roughness of the sea-mean wave height to 0.6 meters instead of 0.25 meters, the entire pattern is considerably reduced due to an increase of the diffuse scattering over specular coefficient.

In Figure 4.8 we want to show the detection contour of a radar with appreciably higher frequency (1000 MHz instead of 100 MHz). The elevation angle is also reduced since the beamwidth is proportional to  $\frac{\lambda}{D}$ , where  $D$  is the physical dimension of the antenna. The plot is carried out for a perfectly smooth sea and horizontal polarization. We can see the effect of the symmetrical antenna pattern on the detection contour. The effects of higher frequency are [Ref. 5,9]:

- 1) the lobes are finer,
- 2) more closely spaced, and,
- 3) the first lobe is at lower elevation angle.

The effect of sea roughness at high frequencies is slightly different from that at low frequencies. Figure 4.9 uses the same radar as in Figure 4.8 except mean sea wave height is changed from 0 to 0.6 meters. At high frequency the roughness of sea has a stronger effect especially on the higher angle lobes. An additional effect which is not included in the program of these plots is that nulls are partially filled in this case, especially in the side lobes. The multipath effect disappears due to a considerable decrease in the specular reflection coefficient  $\rho_s$  at high angles [Ref. 10].

If the signal is spread over a band of frequencies, the nulls may occur around one frequency and not in another frequency, resulting in a decrease in fading time. By "spreading" the multipath effect over a wide band (whitening it, in a sense) we can reduce the effect of no detection at nulls which occur for radars operating at a single frequency.



# HORIZONTAL POLARIZATION

WAVELENGTH = 3.00 METERS  
 ANTENNA HT = 20.00 METERS  
 MEAN WAVE HT = 0.00 METERS

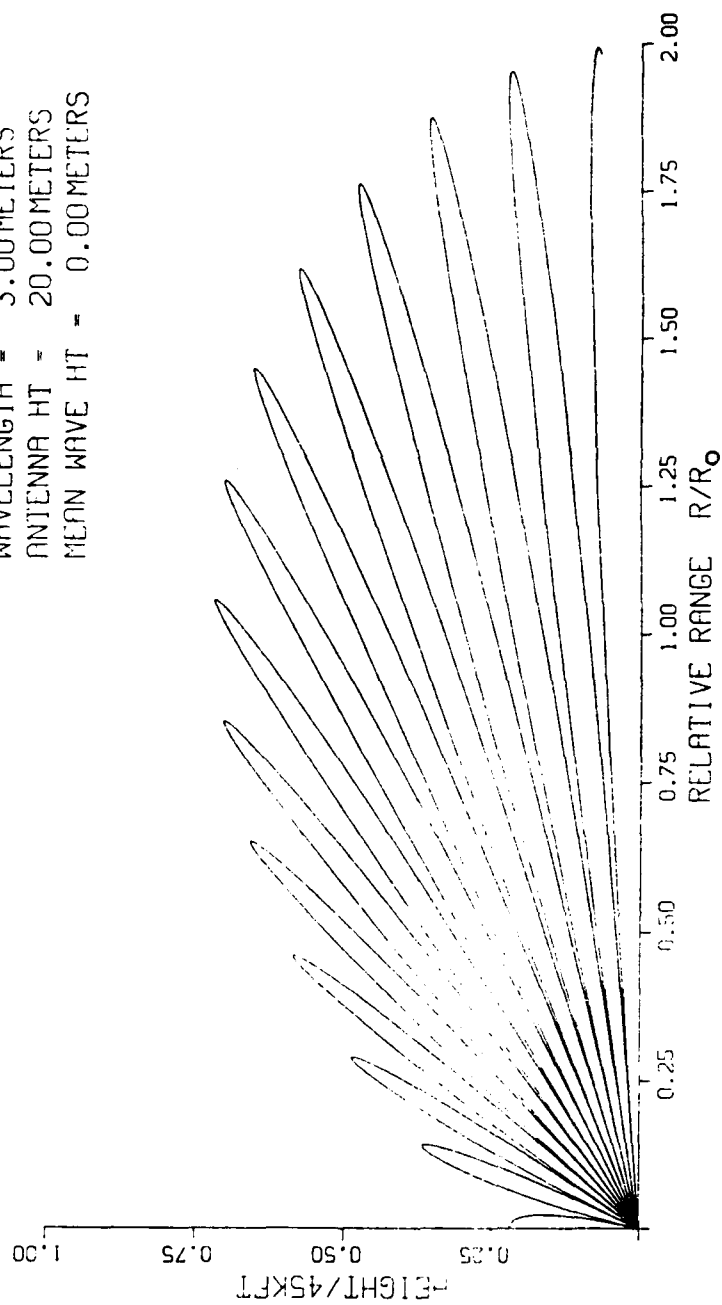


**Figure 4.5: Detection Pattern of Rectangular Antenna with Uniform Field Distribution.**

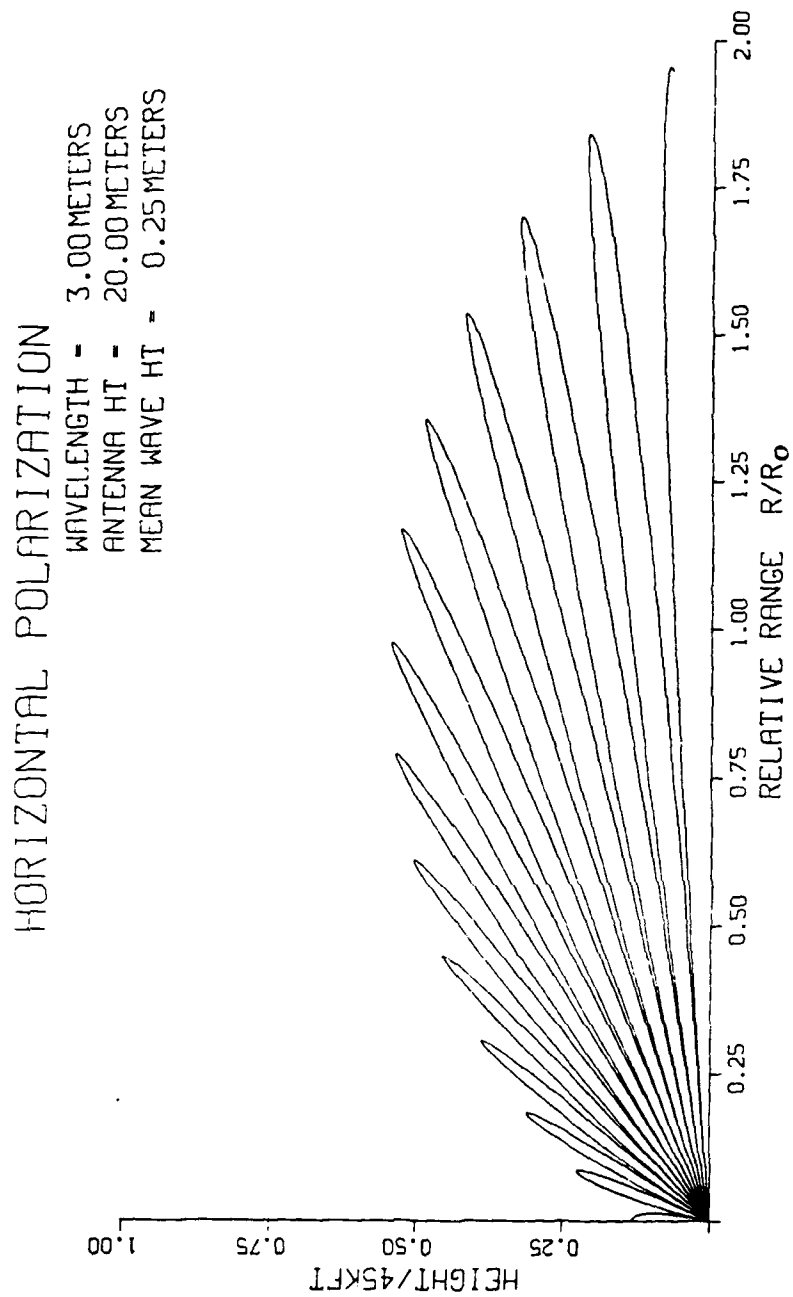


**Figure 4.6: Detection Pattern Same Parameters as Figure 4.5 except Including the Scattering Coefficient Effect.**

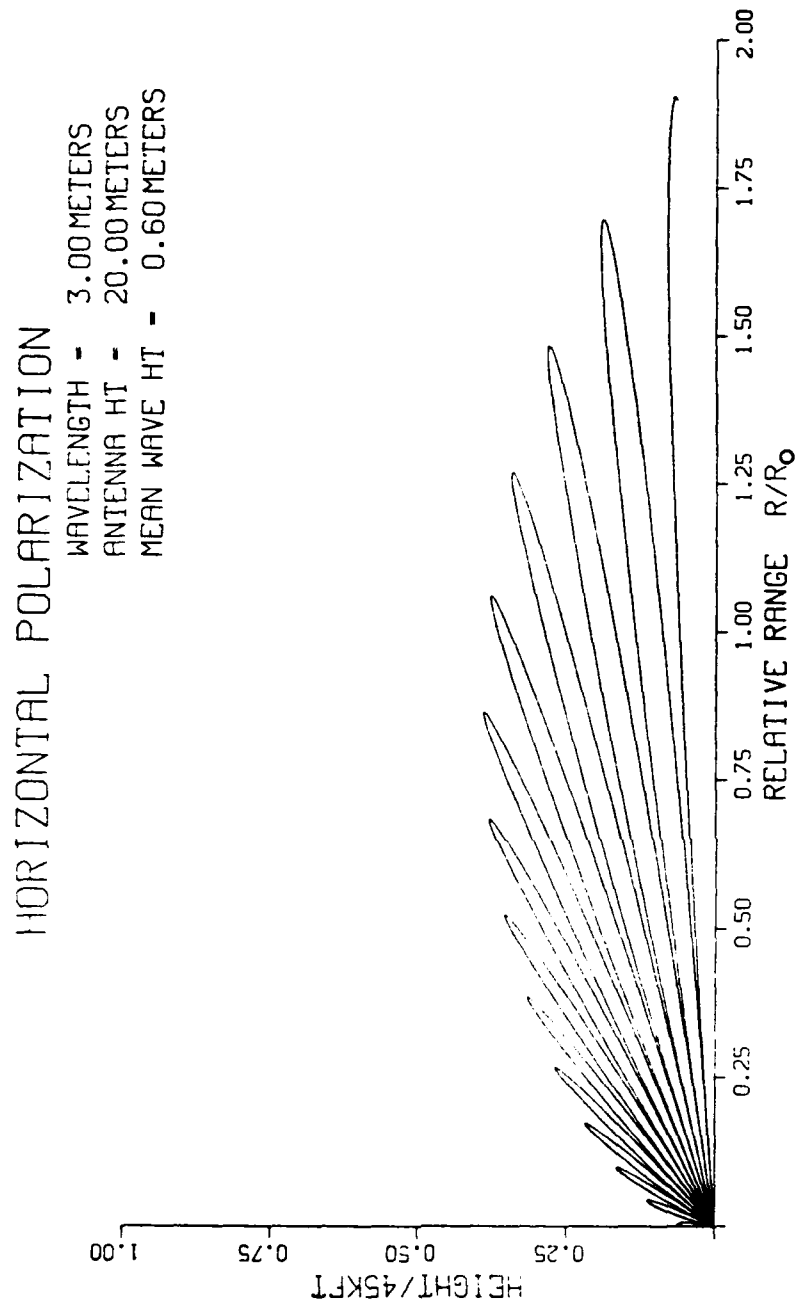


**Figure 4.7: Detection Pattern Showing the Effect of Sea Roughness.**

Also at 1000 MHz if we change the polarizations to vertical, the lobes magnitudes would reduce at elevation angles higher than  $2^\circ$  as can be inferred from the  $\rho_V$  curve in Figure 3.4.

Some typical Naval search radars operate in the S band (2–4 GHz). Figure 4.10 illustrates this practical detection pattern at ideal conditions for lobing phenomena over a perfectly smooth sea.

A very useful way to analyze the multipath effects on the detection capability of a radar is a plot of the received signal versus range. This method is especially used to analyze targets flying at constant altitude towards a radar. This situation can simulate the detectability of an anti-ship missile approaching a ship.

This plot is more convenient for analysis of detection capability of targets in the first lobe (very low altitude targets) within the horizon range. In this plot  $-93$  dBm is the minimum detectable signal (MDS). Signals below this level will not be detected. We see that the “dips” in echo signal due to multipath are narrower and more frequent as range decreases. This effect has been experimentally verified.

We will only mention here that surface reflection causes errors in height measurements. This is because the reflected wave can be considered by the radar as an echo signal from a target located at the same range as the actual target but at the opposite height, i.e., the image of the actual target. When constructive interference occurs, the radar will measure the mean value of the elevation angles of both the actual and the image targets, resulting in a severe error in height measurement.

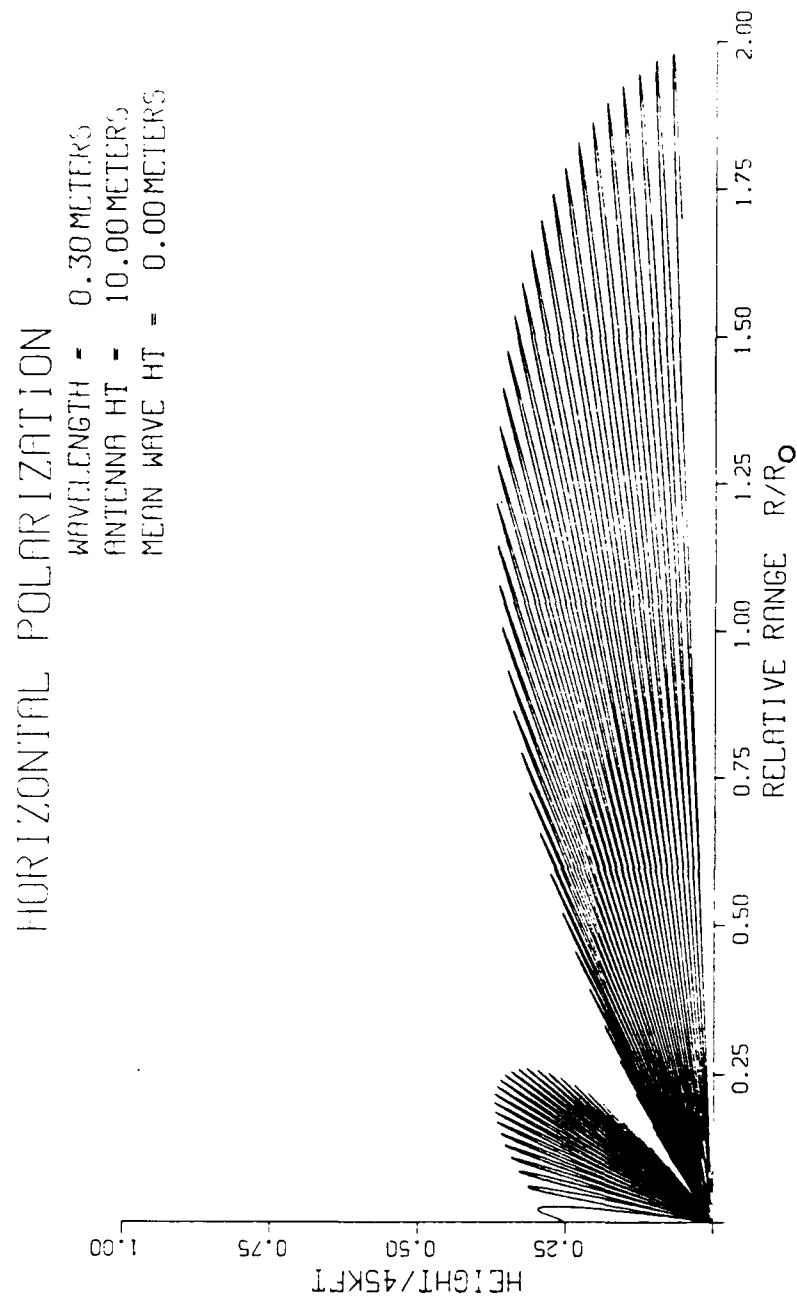


**Figure 4.8: Detection Pattern for Higher Frequency (1000 MHz) and Narrower Vertical Beam Width.**

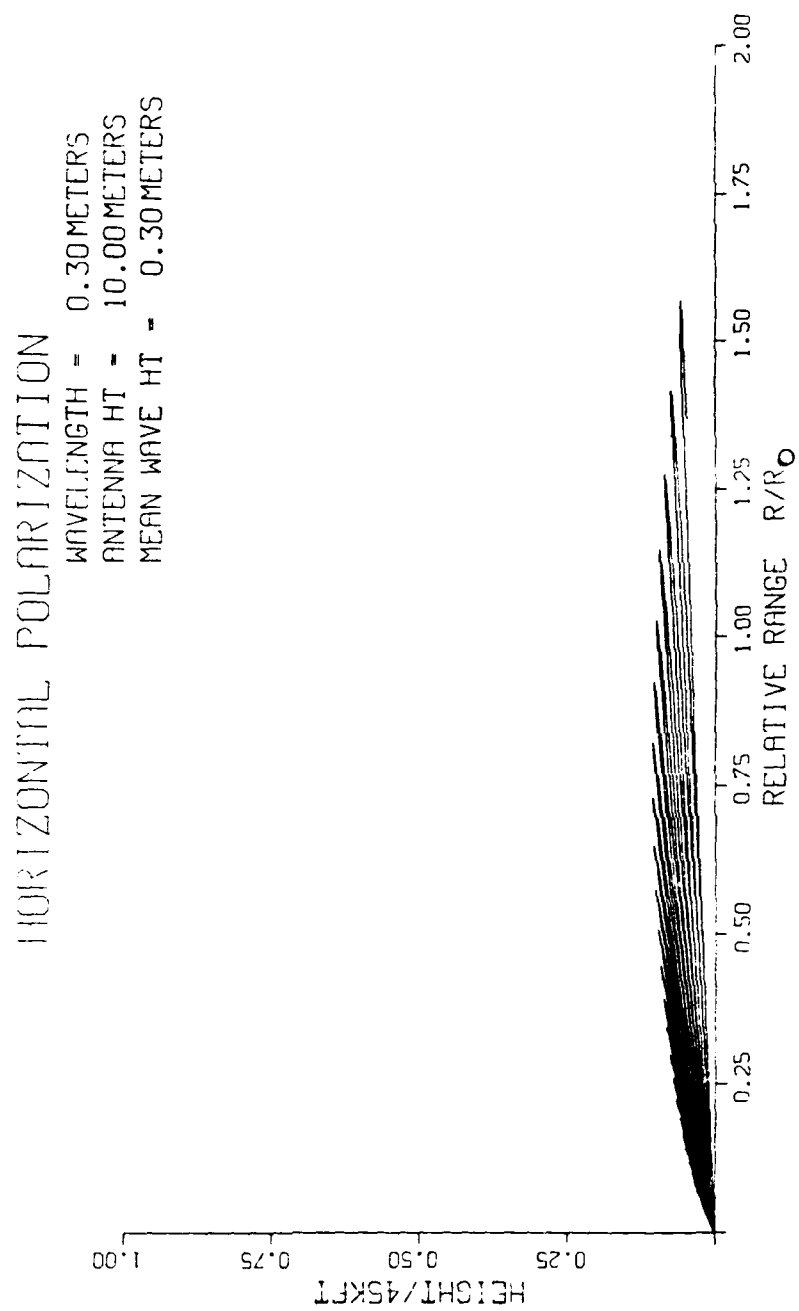


**Figure 4.9: Effect of Sea Roughness on a 1000 MHz Detection Pattern of a Radar.**

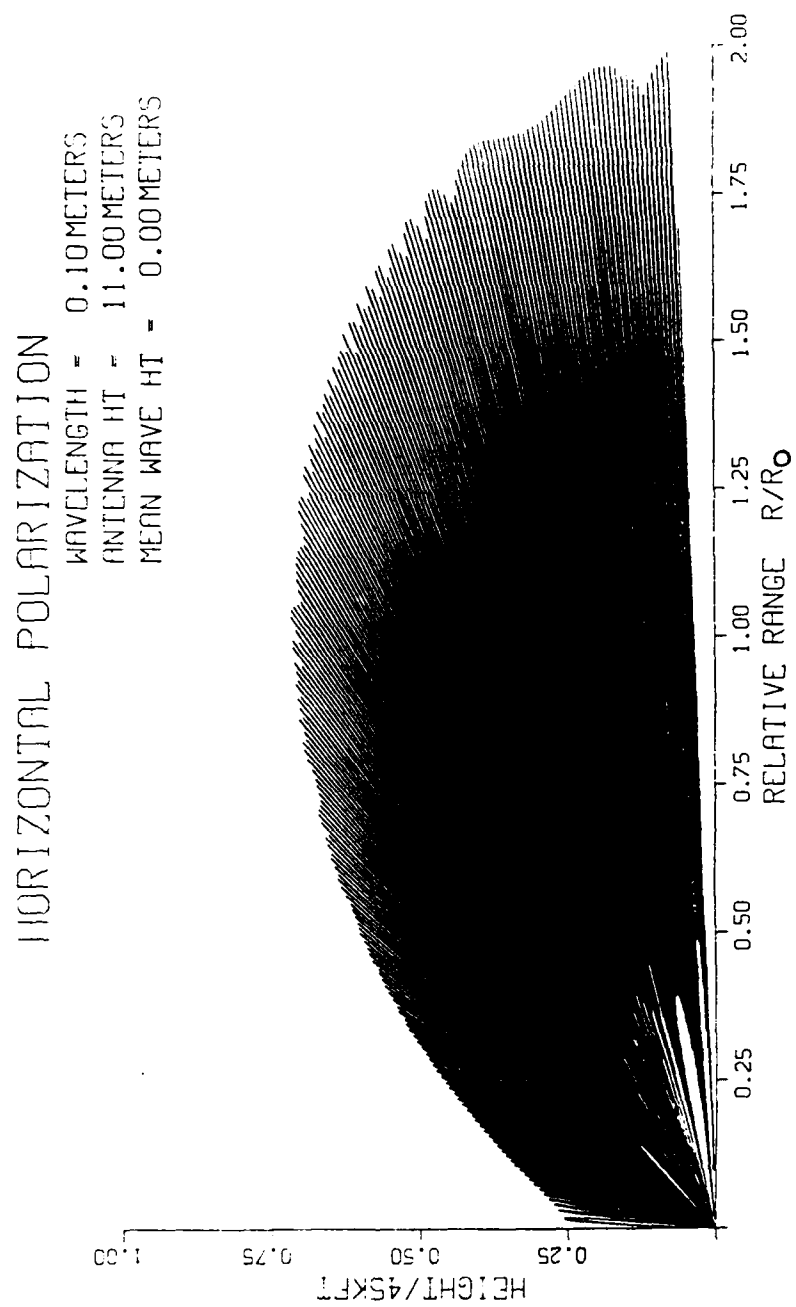


**Figure 4.10: Detection Pattern under Lobing Effect for S Band Naval Surface Searching Radar.**

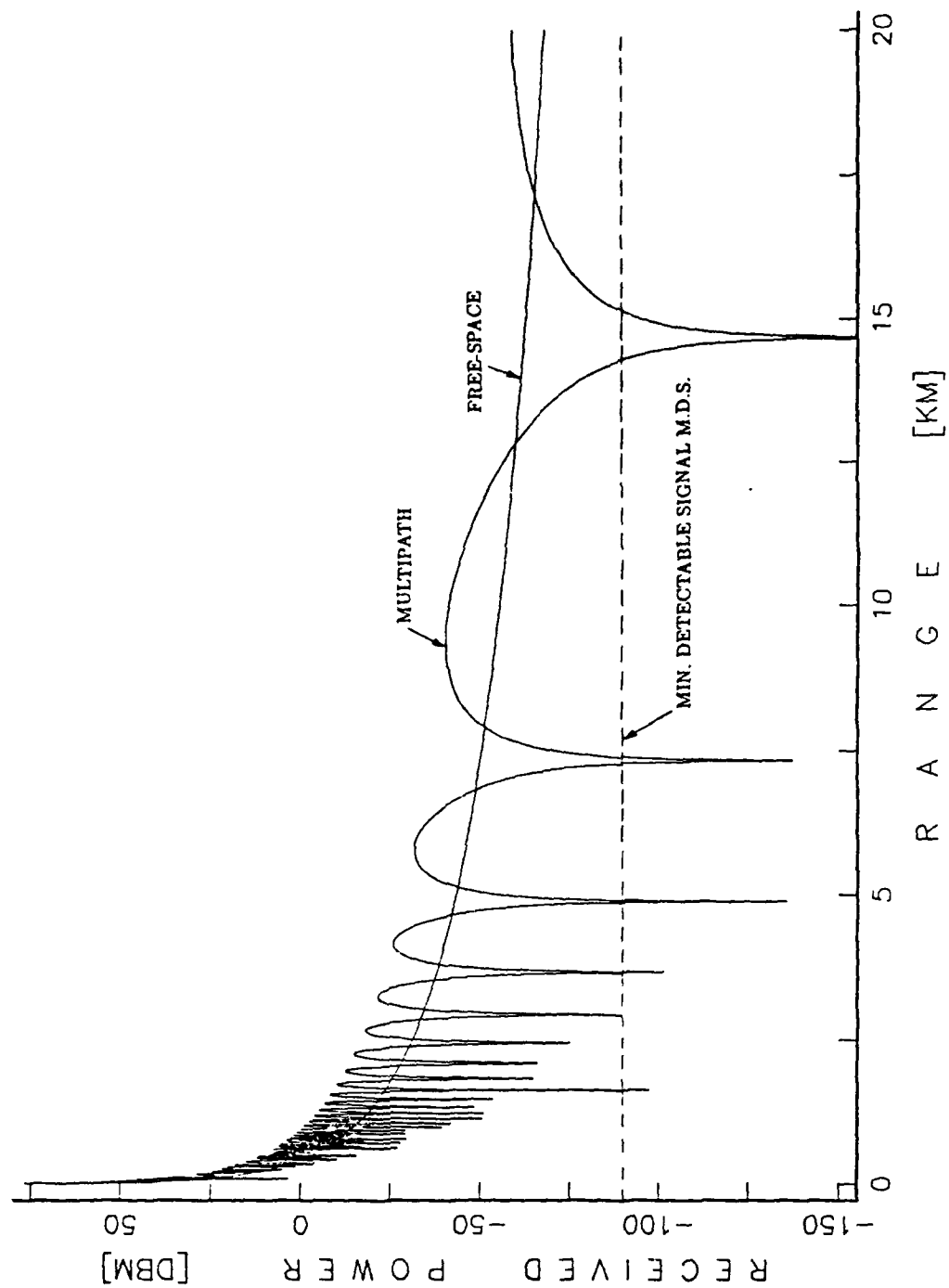


**Figure 4.11: Received Signal Relative to Minimum Detectable Signal, for Multipath and Free Space Conditions.**



## H. SUMMARY AND CONSEQUENCES

We have seen in this chapter that the specularly reflected field may, if it is comparable in amplitude to the direct propagating field, produce deep fades in the total field through interference. The diffused field has much less effect on the fading when it occurs.

Atmospheric refractive layers can cause many different path rays. In this chapter we considered only the interference caused by the direct ray reflected from sea surface, with no effect of the atmospheric refractive layer.

The main parameters affecting the detection pattern of a radar are:

- 1) Antenna height: Increasing the antenna height increases the number of lobes with less uncovered spaces in the detection pattern. The first beam is lowered resulting in better detection of low altitude targets.
- 2) Transmitting frequency: Higher propagating frequency will produce a covering pattern with finer and more lobes. The lowest lobe will be considerably lower.
- 3) Polarization: The lobing phenomenon is more prominent for the horizontal polarization since the magnitude and phase of the reflected waves are more closely correlated to those of the incident wave. For vertical polarization the reflection coefficient (magnitude and phase) depends strongly on the grazing angle and decreases at higher angles and frequencies, resulting in a decreased detection pattern. The effect is stronger at higher frequencies (above 1000 MHz).
- 4) How to decrease the lobing phenomena? For some operational applications, it is possible to overcome the multipath effect. For example, in the detection of low altitude targets and in active jamming, fading is not desirable. Some means of reducing the fading phenomenon are:

a) use of spread spectrum techniques (such as frequency agility or hopping), resulting in a spread of fading time over the spectrum.

b) transmit vertical polarization at frequencies above 1000 MHz. At very high frequencies (35 GHz), the multipath effect is minimal.

The above parameters can be easily controlled by the radar designer.

## **V. ANOMALOUS ATMOSPHERIC PROPAGATION**

### **A. INTRODUCTION**

In the previous chapters, we considered and discussed mainly the characteristics and effects of earth's surface, i.e., sea surface, assuming normal atmospheric conditions.

In this chapter we will consider propagation under abnormal conditions called ducting or anomalous propagation caused by rapid decrease of the refraction index, especially in warm areas such as the Mediterranean Sea. This phenomenon considerably extends the detection range of a radar within the ducting layer compared to horizontal free space range. On the other hand, from conservation of energy, the increase range in one path will cause a decreased range in another path, resulting in holes of detection outside the ducting layer.

We will consider mainly the surface or evaporation duct because it is the most likely one above a sea surface. Refraction losses are also discussed. We will end with some conclusions for radars operating in a duct.

### **B. TROPOSPHERIC REFRACTION**

Electromagnetic waves propagating in the troposphere do not travel in straight lines; instead they tend to bend, due to refractivity of the troposphere, which is related to its dielectric constant. This dielectric constant is a function of temperature, pressure, and water vapor content of the air. [Ref. 9]

The two main effects of this phenomenon on radar performance are:

- 1) An increase in the maximum range of propagation is increased, and,
- 2) errors in measurements of elevation angle.

Figure 5.1 illustrates a simplified scheme of these effects.

### 1. Refraction Effect

Refraction or bending of electromagnetic waves in the atmosphere is caused by the variation of the velocity of propagation with height.

The index of refraction is the ratio of the velocity of propagation in free space to that in an actual medium. For microwave frequencies propagating in the troposphere, which contains water vapor, the refractivity can be calculated by [Ref. 5]:

$$N = (n - 1)10^6 = \frac{77.6p}{T} + \frac{3.73 \times 10^5 e}{T^2}, \quad (5.1)$$

where  $p$  is the barometric pressure in mbars,  $e$  is the partial pressure for water vapor in mbars and  $T$  is the absolute temperature in degrees K. The refractivity  $N$  is used instead of the index of refraction  $n$  because it is a more convenient unit when dealing with propagation. The index of refraction normally decreases with height since the barometric pressure  $p$  and the water vapor content  $e$  decrease much faster with height than the temperature  $T$ .

The index of refraction is also given by:

$$n = \frac{c}{v_g}, \quad (5.2)$$

where  $c$  is the velocity of light in a vacuum ( $3 \times 10^8$  m/sec) and  $v_g$  is the velocity of the propagating wave in the actual medium. Near the surface of earth the index of refraction is 1.0003. Since  $n$  decreases with altitude the velocity of propagation increases with altitude. According to Snell's law the propagating wave tends to bend towards the lower velocity. The result is an increase in propagating range.

Since the refraction index  $n$ , varies with height, it can be shown from Snell's law for spherical geometry that the factor  $\hat{k}$  is varying with height and has the form of [Ref. 3,5]:

$$\hat{k} = \frac{1}{1 + r_e(dn/dh)}, \quad (5.3)$$

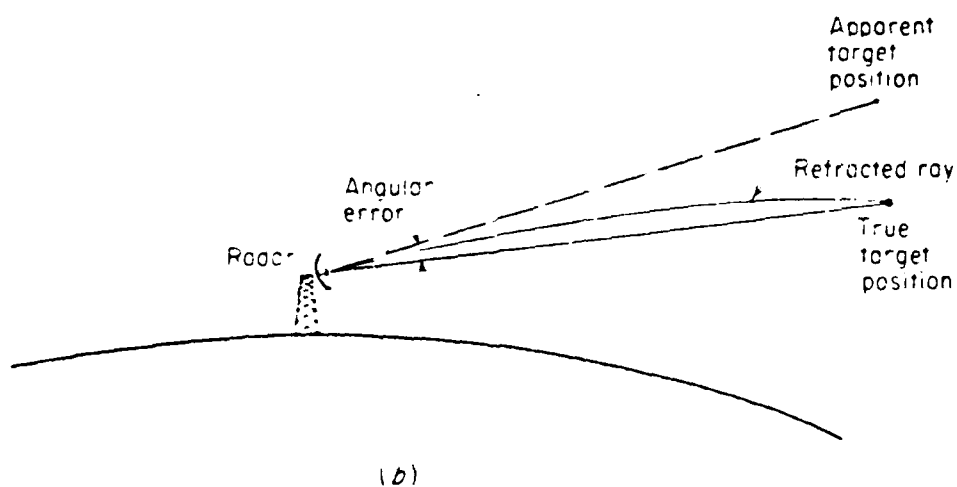
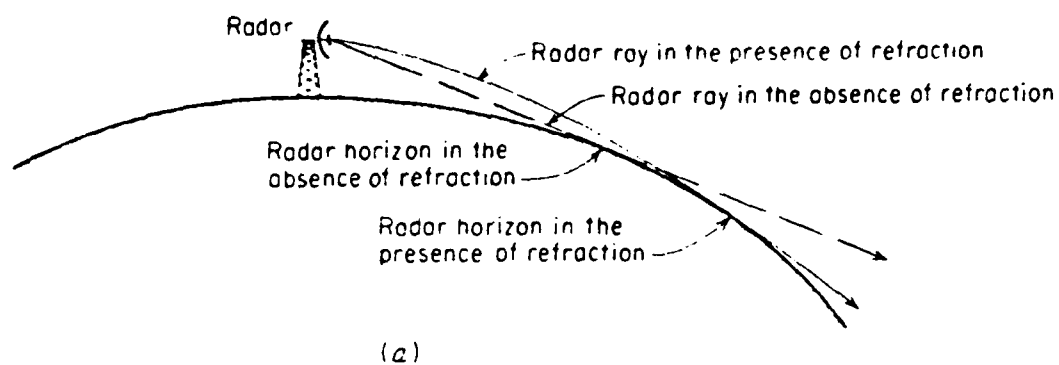


**Figure 5.1: (a) Extension of Radar Horizon; (b) Elevation Angular Error**  
**[Ref. 5].**

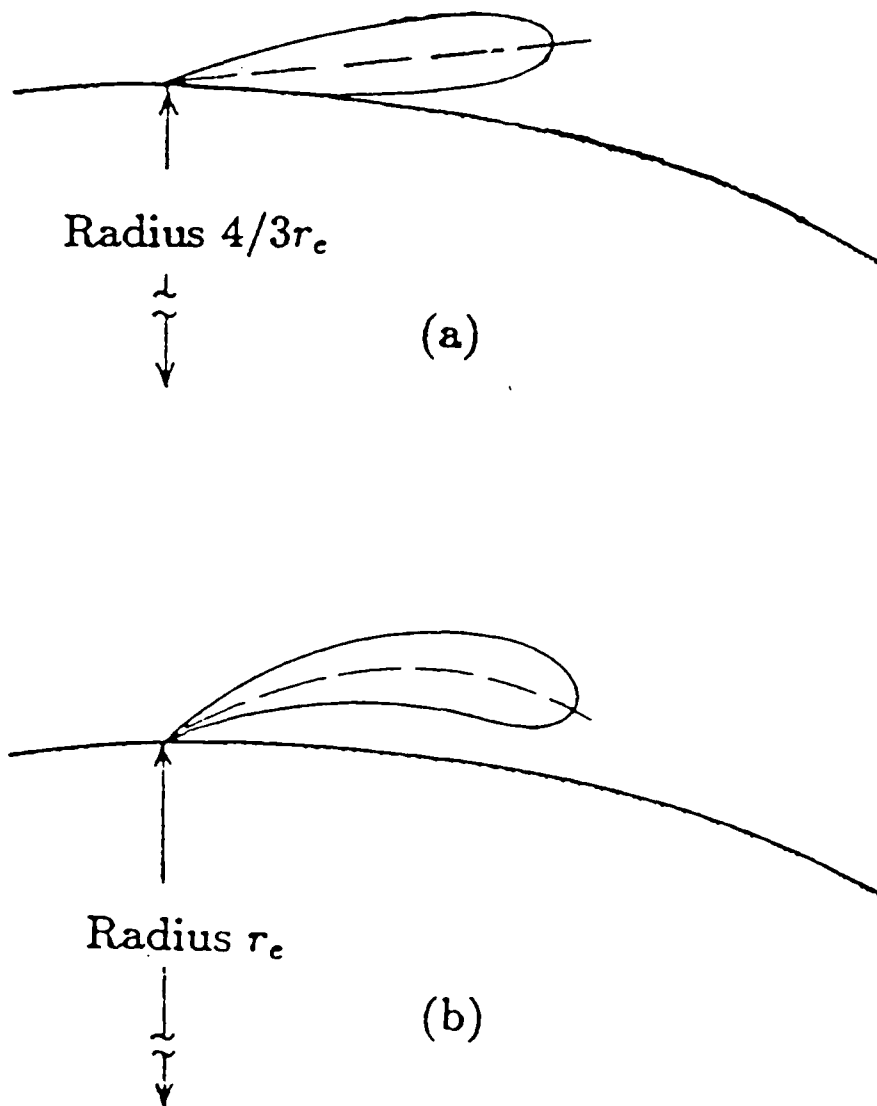


**Figure 5.2: (a) Bent Beam due to Refraction; (b) Straight Line Propagation with Effective Earth Radius  $4/3r_e$  [Ref. 5].**

where  $dn/dh$  is the gradient of the index of refraction with height.

In Chapter III we considered the refraction effect by increasing the earth's radius by a constant factor of  $4/3$ , to obtain the effective earth radius for straight line propagation. This is only an average radius and should not be used for anything other than general calculations. It gives a rough idea of refractivity under normal atmospheric conditions. Figure 5.2 shows the replacement of earth radius by an effective radius of  $4/3r_e$  assuming a homogeneous atmosphere and constant gradient of index of refraction with height.

The variation of index of refraction with height was found to be an exponential function rather than a linear function as assumed for  $\hat{k} = 4/3$ . The exponential model for refractivity is given by [after Ref. 5]:

$$N_s = N_e \exp[-C_e(h_T - h_R)], \quad (5.4)$$

where  $N_e$  is the refractivity at the surface of the earth,  $C_e$  is a constant,  $h_R$  is the radar antenna height and  $h_T$  is the target altitude. Use of this refractivity model results in smaller errors in elevation angle measurements of the target.

### C. REFRACTION LOSS

At normal refraction conditions, when the vertical gradient of refractivity is constant ( $\frac{dn}{dh} = \text{const.}$ ), the main effect will be an increased elevation error as measured by the radar. However, another effect, which is considered by Weil 1973 [Ref. 9], is a divergence loss of signal strength that is caused by the refractions of rays from atmospheric inhomogenities. This loss is also known as Lens Effect Loss since the effects caused by the atmosphere are similar to the lens effect.

To illustrate this effect consider a source radiating four rays  $A, B, C, D$  as in Figure 5.3. Without any absorption or refraction disturbances at the distance  $R$ , these four rays will be spread out through an area equal to  $\bar{\delta}^2 R^2$ , where  $\bar{\delta}$  is the angular separation in radians between the rays. Now assume that the rays are propagating under refractive conditions which will cause them to bend rather than to propagate

in straight lines. The rays *C* and *D* have a slightly smaller angle with respect to the vertical gradient of refraction, thereby causing them to bend slightly more than rays *A* and *B*. This will result in a larger spreading area of these rays, causing a decrease in power density. [Ref. 9]

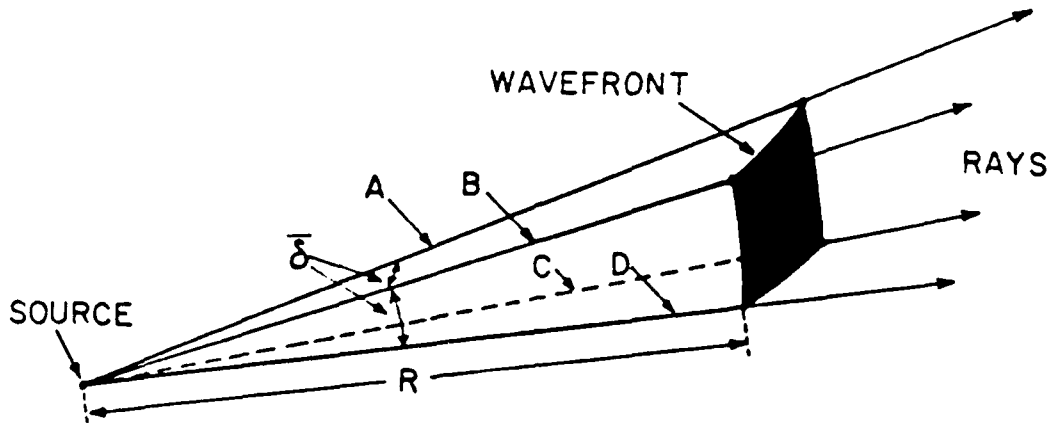


Figure 5.3: Ray Pattern for Refractive Loss Analysis [Ref. 9].

This refractive or lens effect loss, can be calculated by the ratio of wave front areas:

$$L' = \frac{A'}{A}, \quad (5.5)$$

where  $A'$  is the wavefront area under refractive conditions and  $A$  is the free space wavefront area.

Figure 5.4 shows the lens effect loss in dB as a function of the range of propagation with the elevation angle as a parameter. The conclusion from this graph is that, although the lens effect is not large, it is important in the case of long range detection radars trying to detect targets at low altitudes (low angles). At angles higher than  $2^\circ$ , the lens effect loss is seen to be negligible.

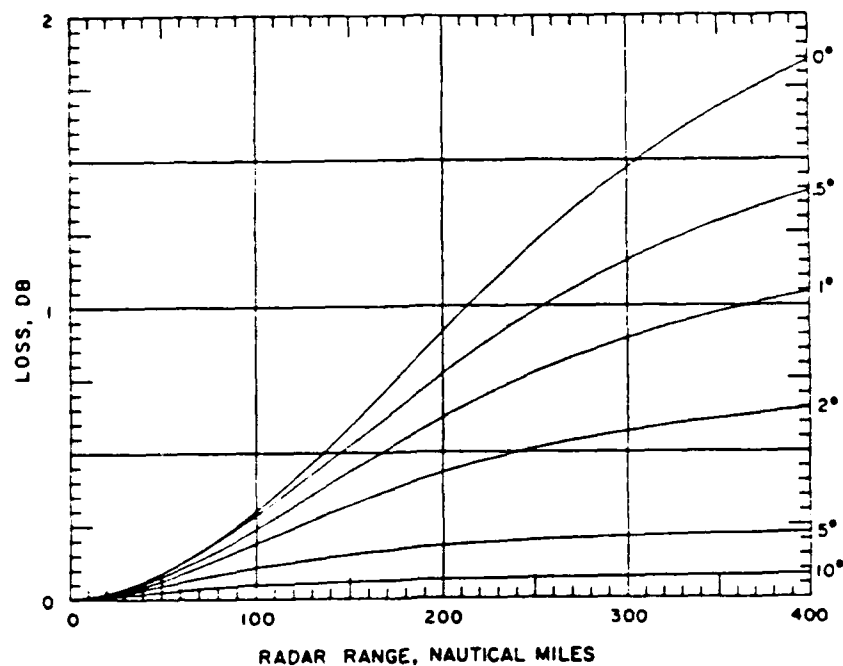


Figure 5.4: Lens Effect Loss as a Function of Elevation Angle vs. Range [Ref. 4].

#### D. PROPAGATION UNDER ANOMALOUS CONDITIONS

Theoretically, under ideal conditions with no attenuation and absorption, the vertical gradient of index of refraction could have a high value causing rays to curve similar to the earth curvature resulting in continued propagation around the earth. The effective radius will be almost infinite if  $\frac{dn}{dh} = -1.57 \cdot 10^{-7} m^{-1}$  allowing horizontal rays to propagate around the earth's curvature with no horizon limits. This condition is called "ducting," in which the electromagnetic ray is "trapped." These conditions can occur only within an atmospheric layer with a finite thickness.

Values of vertical refractive gradient for normal and abnormal propagation are known to be [Ref. 5]:



- 1) For normal atmospheric refraction  $0 < \frac{dn}{dh} < -0.787 \cdot 10^{-7} m^{-1}$  or  $1 \leq K \leq 2$ .
- 2) For superrefraction conditions  $-0.787 \cdot 10^{-7} < \frac{dn}{dh} < -1.57 \cdot 10^{-7} m^{-1}$  or  $2 < K \leq \infty$ .

Ducting occurs when  $\frac{dn}{dh} > -1.57 \cdot 10^{-7} m^{-1}$ . This phenomenon can be compared to a leaky waveguide. There are places along the layer in which the index of refraction increases with altitude instead of decreasing, causing the ray to bend upwards instead of downwards. In spite of the "leakage," ducting usually increases tremendously the horizontal detection range of radars.

Once duct conditions are fulfilled, the refractive index within the duct is greater than the threshold for ducting, resulting in the ray curving down in a curvature larger than that of earth's surface. If the surface is water, some specular reflection will occur. Since the ray is trapped, this process will proceed continuously within the duct as shown in Figure 5.5. It is shown in the figure that there is a critical elevation angle at which the ray propagates within the ducting layer. Beyond this elevation angle, the rays will propagate out of the layer. This critical angle is usually less than  $0.5^\circ$  meaning that the rays are almost parallel to the surface. [Ref 9]

This type of duct with a low layer above surface is called a surface duct, or evaporation duct, if it occurs above water surface. A duct which occurs at higher layers is called an elevated duct. [Ref. 5,9,13]

The evaporation duct usually occurs within a few tens to almost a hundred feet above the sea surface. The duct effect can be interpreted as "forcing" the wave to propagate in one dimension (horizontal) rather than in the two dimensions under normal conditions (horizontal and vertical). This results in power density spreading as the inverse first power of the range ( $1/R$ ) instead of  $1/R^2$ . In two way propagation radar, the receiving energy will be proportional to  $1/R^2$  under ducting conditions instead of the  $1/R^4$  in free space. The result is that for a radar and a target within the ducting layer, the detection range will be much beyond the "horizon" range of free space (see Fig. 5,6). [Ref. 9, 13]

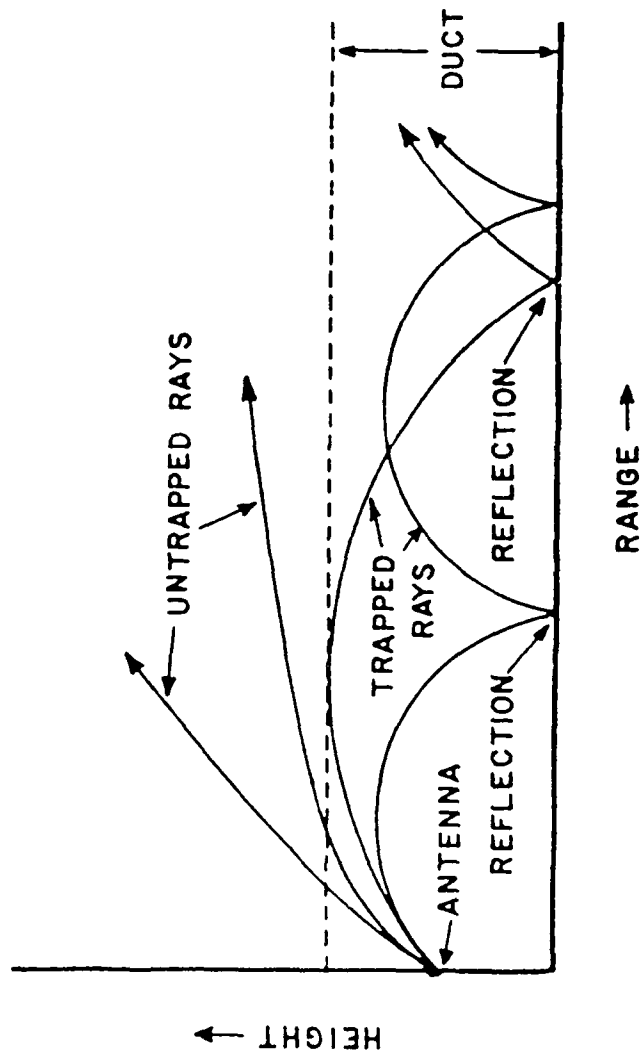


Figure 5.5: Ray Propagation Pattern under Ducting Conditions [Ref. 9].

Though there are losses caused by absorption and leakage, the ducting phenomena has an effect of increasing the detection range within the layer. This extended detection range occurs because more energy is directed into the ducting layer by refraction, while less energy will propagate in other directions causing "holes" or poor detection in areas outside of the ducting layer. We can conclude that a surface or evaporation duct favors detection of surface or sea skimming targets, and does not favor the detection of targets with elevation angles greater than  $1^\circ$ .

### E. SURFACE DUCT CHARACTERISTICS AND ATMOSPHERIC RELATIONSHIP

As mentioned in Chapter V, Section A.1, the refraction index decreases with height in normal atmospheric conditions. Under certain conditions, especially in subtropical regions, there is a warm layer over a colder layer which means that temperature increases with height instead of decreasing with height. This, together with normal rapid decrease of pressure and evaporation, results in a more rapid decrease of refraction index than under normal conditions. Such ducts are common in tropical and semitropical areas over cold sea water with a maximum height of at most, a few hundred feet. [Ref. 3,9]

Another type of duct, the evaporation duct, is due to evaporation of moisture from the sea surface. This duct is usually lower, 20-60 ft on the average, and is more reliable than the previously discussed duct. This type of duct is common in the warm areas of the globe such as the Mediterranean Sea, for instance.

The maximum wavelength of an electromagnetic wave able to propagate within a duct depends on its thickness  $\hat{d}$ . A duct could be thought of as a high pass filter allowing only the higher frequencies (shorter wavelength) to propagate abnormally. The maximum wavelength that can propagate in evaporated duct with thickness  $\hat{d}$  is given by [Ref 5]:

$$\lambda_{\max} = 2.5 \left( -\frac{dn}{dh} \right)^{1/2} \hat{d}^{3/2}. \quad (5.6)$$

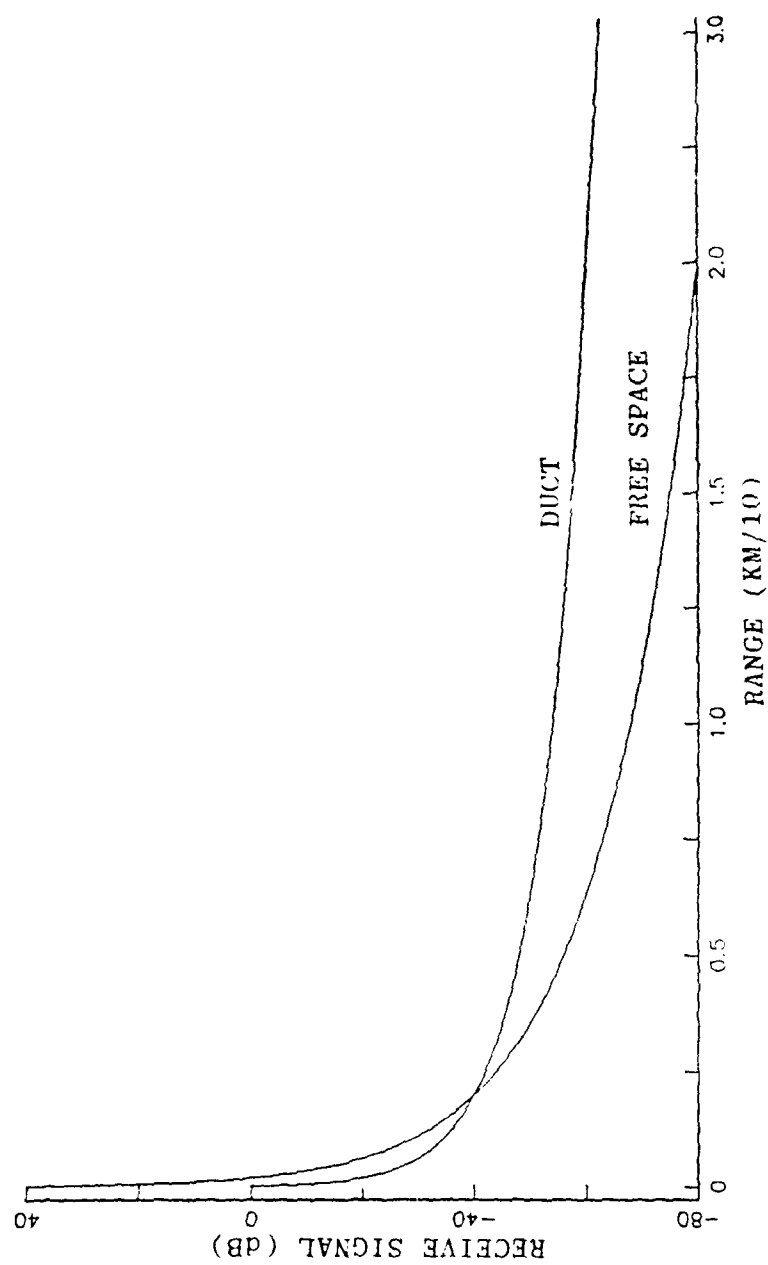


**Figure 5.6: Relative Received Signal Under Duct and Free Space Conditions.**

For an X band radar ( $\lambda = 3$  cm) the required thickness for ducting to occur, would be 10 m. Since ducting layers are not very thick, ducts will usually occur for higher microwave frequencies.

Compared with waveguides, the "cut-off wavelength" for a duct is not so strict. Modes with "harmonic wavelength" can also be propagated by ducts. [Ref. 5]

## **F. CONCLUSIONS OF ANOMALOUS PROPAGATION**

Finally the following points should be considered when designing and/or operating a radar in anomalous propagating conditions:

- 1) Evaporation duct, when used with the appropriate height of antenna and wavelength, can extend the detection for surface or low flying targets considerably beyond the expected range with normal atmospheric conditions.
- 2) The extended horizontal detection range will cause reduced range or holes in detection at other elevated angles. This follows from conservation of energy. This can cause severe coverage problems for air surveillance and early warning radars.
- 3) Usually radar is designed under the assumption that clutter is likely only in the range close to the radar. In ducts, clutter is likely also at longer ranges, resulting in a signal-to-clutter problem for radars without techniques to cancel it (such as pulse staggering against second time around clutter.)

## **VI. SUMMARY AND CONCLUSIONS**

### **A. SUMMARY**

In this study we have tried to quantify the propagation characteristics of an electromagnetic wave through material and media boundaries. Random irregularities of the sea surface, the so-called sea roughness, have been investigated and included in the specular and diffused reflection coefficients. The curvature of the earth's surface is taken into account by way of an effective radius. These parameters were used to compute the detection performance contours of a typical microwave search radar. The multipath effect appears as a lobing factor on the detection range. Further, the effects of anomalous propagation through the atmosphere are also studied. The work illustrates that the propagating medium has a significant effect on the detection range.

### **B. CONCLUSIONS AND RECOMMENDATIONS**

The results of this study show that the reflected field from the sea surface interferes with the direct field, and depends on wavelength, polarization, sea state, angles of incidence, and the electric properties of the sea surface.

By appropriate design and operation of the radar, we can have some control on the detection pattern.

Frequency and/or spatial diversity, of the transmitting frequency and antenna heights respectively, were proved to be very effective in "filling up" dips in the receiving signal caused by multipath. Also, increasing the frequency and antenna height lowers the first lobe of the detection contour, for better detection of targets at low grazing angles.

In areas such as the Mediterranean and the Red Seas, abnormal atmospheric conditions for propagation are very common for most parts of the year. In order to gain the benefit of the ducting phenomena one must predict the thickness of the ducting layer.

By using appropriate antenna height and wavelength, detection of targets within the ducting layer are maximized. Further studies should be made for predicting ducts more accurately so that one can rely on this phenomena.

## APPENDIX: DERIVATION OF ELLIPSES FOR FRESNEL ZONES

To derive the equations of the ellipsoid it is easier to change coordinates to  $x', y', z'$  by tilting the  $x$  coordinate by the angle of  $\theta$  in order to align the coordinate with  $R$  (see Figure 2.3).  $y'$  will be parallel to  $y$  and  $z'$  is obviously orthogonal to the  $x'y'$  plane [Ref. 3,4].

The expressions for the new coordinate systems  $x', y', z'$  are [Ref. 4]:

$$x' = \left(x - \frac{r}{2}\right) \cos \theta + \left(z - \frac{z_1 + z_2}{2}\right) \sin \theta, \quad (\text{A.1})$$

$$y' = y, \quad (\text{A.2})$$

$$z' = -\left(x - \frac{r}{2}\right) \sin \theta + \left(z - \frac{z_1 + z_2}{2}\right) \cos \theta. \quad (\text{A.3})$$

For given  $\delta$  the equation of the ellipsoid is:

$$a^2(y'^2 + z'^2) + b^2x'^2 = a^2b^2. \quad (\text{A.4})$$

where

$$a = \frac{r \sec \theta + \delta}{2}, \quad (\text{A.5})$$

$$b = \frac{1}{2} \sqrt{\delta^2 + 2r\delta \sec \theta}. \quad (\text{A.6})$$

and

$$\tan \theta = \frac{z_2 - z_1}{r}. \quad (\text{A.7})$$

We are interested in the Fresnel zones in the  $xy$  plane transferring the ellipsoid Equation A.4 back into  $x, y, z$  coordinates with  $z = 0$  in the transformation equations, we get a family of ellipsoids:

$$\frac{a^2b^2 (b^2 \cos^2 \theta + a^2 \sin^2 \theta - c^2)}{b^2 \cos^2 \theta + a^2 \sin^2 \theta} = \left(x - \frac{1}{2}r - p\right)^2 (b^2 \cos^2 \theta + a^2 \sin^2 \theta + a^2y^2), \quad (\text{A.8})$$



where

$$c = \frac{z_1 + z_2}{2}, \quad (\text{A.9})$$

$$p = -\frac{c(a^2 - b^2) \sin \theta \cos \theta}{b^2 \cos^2 \theta + a^2 \sin^2 \theta}. \quad (\text{A.10})$$

Equation 2.5 represents an ellipse corresponding to a given  $\delta$ , the center of the ellipse is on  $x$  axis and is given by:

$$x_0 = \frac{r}{2} \left[ 1 - \frac{\left( \frac{z_2 - z_1}{r} \right)^2}{(\delta/r + \sec \theta)^2 - 1} \right]; \quad y_0 = 0. \quad (\text{A.11})$$

By setting  $x = x_0$  the semiminor axis is:

$$y_1 = \pm b \sqrt{1 - \frac{c^2}{b^2 \cos^2 \theta + a^2 \sin^2 \theta}}, \quad (\text{A.12})$$

or

$$y_1 = \pm \frac{r}{2} \sqrt{\left( \frac{\delta}{r} \right)^2 + \frac{2\delta}{r} \sqrt{\left( \frac{z_1 - z_2}{r} \right)^2}} \times \sqrt{1 - \frac{(z_1 + z_2)^2}{\left[ \frac{\delta}{r} + \sqrt{1 + \left( \frac{z_2 - z_1}{r} \right)^2} \right]^2 - 1}}. \quad (\text{A.13})$$

By setting  $y = 0$  the semimajor axis is derived:

$$x_1 = x_0 \pm y_1 \frac{a}{\sqrt{b^2 \cos^2 \theta + a^2 \sin^2 \theta}}. \quad (\text{A.14})$$

Substituting Equations A.5, A.6, and A.7 into Equation A.14 yields:

$$x_1 = x_0 \pm y_1 \sqrt{1 + \frac{1}{\left[ \frac{\delta}{r} + \sqrt{1 + \left( \frac{z_2 - z_1}{r} \right)^2} \right]^2 - 1}}. \quad (\text{A.15})$$

For practical computations these equations can be simplified by assuming that  $z_1, z_2$  and the path difference of  $\delta$  are much smaller than  $r$ . This yields to:

$$\left[ \frac{\delta}{r} + \sqrt{1 + \left( \frac{z_2 \pm z_1}{r} \right)^2} \right]^2 - 1 \approx \frac{2\delta}{r} + \left( \frac{z_2 \pm z_1}{r} \right)^2 \ll 1. \quad (\text{A.16})$$

## LIST OF REFERENCES

1. Beckman, P., and Spizzichino, A., *The Scattering of Electromagnetic Waves from Rough Surfaces*, Macmillan Company, 1963.
2. Long, M. W., *Radar Reflectivities of Land and Sea*, Lexington Books, 1975.
3. Kerr, D. E., *Propagation of Short Radio Waves*, McGraw-Hill Book Company, Inc., 1951.
4. Rome Air Development Center, Griffis Air Force Base, N. Y., In-House Report no. RADC-TR-84-159, *The Use of the Glistening Surface Concept in Rough Surface Scattering*, by R. J. Papa, J. F. Lennon, and R. L. Taylor, July 1984.
5. Skolnik, M. I., *Introduction to Radar Systems*, 2nd ed., McGraw-Hill Book Company, Inc., 1980.
6. Naval Research Laboratories Memo. Report no. 6098, *Models for Electromagnetic Scattering from the Sea at Extremely Low Grazing Angles*, by L. B. Wetzel, December 1987.
7. Barton, D. K., and Ward, H. R., *Handbook of Radar Measurement*, Artech House, 1984.
8. Private communication between Dr. R. D. Hayes, Naval Postgraduate School, Monterey, CA and the author, May 1988.
9. Blake, L. V., *Radar Range - Performance Analysis*, Artech House, 1986.
10. Nathanson, F. E., *Radar Design Principles*, McGraw-Hill Book Company, Inc., 1969.
11. Naval Research Laboratories Report no. 3163, *Detection Ranges of Low Altitude Targets Over the Sea Surface*, by J. K. Hasiao, November 1975.
12. Beard, C. I., "Coherent and Incoherent Scattering from the Ocean," *IRE Transactions on Antennas and Propagation*, v. AP-9, September 1961.
13. Meeks, M. L., *Radar Propagation at Low Altitudes*, Artech House, 1984.
14. Weil, T. A., "Atmospheric Lens Effect; Another Loss for the Radar Range Equation," *IEEE Transactions on Aerospace and Electronic Systems*, Vol. AES-9, No. 1, pp. 51-54, January 1973.

## BIBLIOGRAPHY

Naval Research Laboratories Report no. 6930, *A Guide to Basic Pulse-Radar Maximum-Range Calculation*, by L. V. Blake, December 1969.

Lincoln Laboratories Technical Report no. 373, *MA Influence of the Earth's Surface on Radar*, by N. I. Durlach, January 1965.

Rohan, R., *Surveillance Radar Performance Prediction*, Peter Peregrinus, Ltd., 1975.

Stutzman, W. L., and Thiele, G. A., *Antenna Theory and Designs*, John Wiley and Sons, 1981.

Valenzuela, G. R., "Scattering of Electromagnetic Waves from a Tilted Slightly Rough Surface," *Radio Science*, v. 3, no. 11, November 1968.

## INITIAL DISTRIBUTION LIST

	No. of Copies
1. Defense Technical Information Center Cameron Station Alexandria, VA 22304-6145	2
2. Library, Code 0142 Naval Postgraduate School Monterey, CA 93943-5002	2
3. Chairman, Code 62 Department of Electrical and Computer Engineering Naval Postgraduate School Monterey, CA 93943-5000	1
4. Professor Rama Janaswamy Code 62Js Naval Postgraduate School Monterey, CA 93943-5000	1
5. Professor Robert Partelow Code 62Pw Naval Postgraduate School Monterey, CA 93943-5000	1
6. Professor Daniel C. Bukofzer Code 62Bu Naval Postgraduate School Monterey, CA 93943-5000	1
7. Professor Rudolf Panholzer Code 62Pz Naval Postgraduate School Monterey, CA 93943-5000	1

- |     |   |   |
|-----|---|---|
| 8.  | Professor Gilbert T. Howard<br>Code 012<br>Naval Postgraduate School<br>Monterey, CA 93943-5000   | 1 |
| 9.  | Commodore Micha Ram<br>C/O Naval Attaché<br>Embassy of Israel<br>3514 International Drive, N. W.<br>Washington D. C. 20008                  | 1 |
| 10. | Commodore Arie Rona<br>C/O Naval Attaché<br>Embassy of Israel<br>3514 International Drive, N. W.<br>Washington D. C. 20008                  | 1 |
| 11. | Captain Shaul Horev<br>119 Sea Foam<br>Monterey, CA 93940   | 1 |
| 12. | Major Zeev Snir<br>310 5th Street<br>Monterey, CA 93940   | 1 |
| 13. | Mr Michael Y. Lin<br>Watkins-Johnson International<br>3333 Hillview Ave.<br>Palo Alto, CA 94304   | 1 |
| 14. | Mr. Dubi Grinberg<br>C/O Defense and Armed Forces Attaché<br>Embassy of Israel<br>3514 International Drive, N. W.<br>Washington D. C. 20008 | 1 |
| 15. | Commander Moshe Marom<br>2101 Etna Place<br>Monterey, CA 93940  | 5 |

- |   |   |
|---|---|
| 16. Space and Naval Warfare Systems Command | 1 |
| Code PDW 106                                |   |
| Washington D. C. 22202                      |   |
| 17. Deputy Chief of Naval Operations        | 1 |
| Code NOP-05                                 |   |
| Washington D. C. 20350                      |   |